# High-Energy Astrophysics

Andrii Neronov

October 23, 2017

# Contents

# Chapter 1

# Introduction

The term *"High-Energy Astrophysics"* combines two keywords which determine the scope of the subject.

The "High-Energy" physics conventionally deals with the world of high-energy particles, i.e. particles with energies much higher than the rest energy. For electrons the rest energy is

$$E = m_e c^2 \simeq 5 \times 10^5 \text{ eV} \tag{1.1}$$

(here $m_e = 0.9 \times 10^{-27}$ g is the mass of electron and $c = 3 \times 10^{10}$ cm/s is the speed of light), while for proton it is

$$E = m_p c^2 \simeq 10^9 \text{ eV} \tag{1.2}$$

with the proton mass $m_p = 1.6 \times 10^{-24}$ g. In laboratory conditions here on Earth, the high-energy particles are produced by accelerator machines, like the Large Hadron Collider (LHC) at CERN, in which protons reach energies in the range of 10 TeV. The main goal of the High-Energy Physics research is to understand the fundamental constituents of matter (elementary particles) and interactions between them.

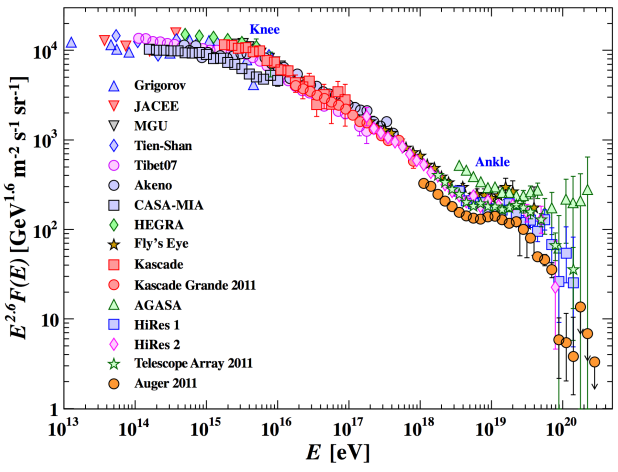


Figure 1.1: The spectrum of cosmic rays measured by different experiments. This log-log scale plot shows the differential flux of particles per unit energy interval, $F(E)$, multiplied by energy $E$ to the power 2.6. From Ref. [4].

Second part of the name High-Energy Astrophysics contains the word *"Astrophysics"* which clearly refers to astronomical observations, typically done using various types of telescopes and aimed at understanding of the properties and mechanisms of activity of different types of astronomical sources, like stars and galaxies.

Combining the two parts into one subject defines the subject of High-Energy Astrophysics as research in the domain of Astronomy, specifically aimed at understanding of the role of high-energy particles and their interactions in the activity of different types of astronomical sources.

The fact that some astronomical objects work as particle accelerators is established based on two types of observational data.

First, we directly detect the high-energy charged particles coming from space in the form of *cosmic rays*. Measurements of the spectrum of cosmic rays (Fig. 1.1) show that the energies of the cosmic ray particles reach $10^{20}$ eV, which is some seven orders of magnitude higher than the maximal energies of protons attained at the LHC.

These particles are produced by some (still unknown) astronomical sources and it is one of the major challenges of modern physics and astronomy to identify these sources. The uncertainty of the sources of cosmic rays constitutes the long-standing *problem of the origin of cosmic rays*. The cosmic rays were first discovered in 1912, so the problem is now 100-year-old.

Next, the information on the presence of high-energy particles in astronomical sources is obtained indirectly, via observations of those sources with telescopes operating at different wavelengths, i.e. with the tools of the *"multi-wavelength astronomy"*. From the early days of the mankind, people have started to do astronomical observations, by looking at the stars on the sky first with the naked eye, and then, starting from Copernicus, with telescopes. Up to the middle of 20th century, the word "astronomical observations" was synonymous to the "astronomical observations in the visible band", because the only type of light sensors used was the human eye, sensitive in the visible range. The visible energy band contains photons in the wavelength range

$$400\text{nm} \leq \lambda \leq 700 \text{ nm} \tag{1.3}$$

This corresponds to a rather narrow range of photon energies $\epsilon = 2\pi\hbar c/\lambda$

$$1.8 \text{ eV} < \epsilon < 3.2 \text{ eV} \tag{1.4}$$

Only astronomical sources emitting photons in this specific energy range were known all this time.

Starting from the end of 1960's, the tools of radio, infrared, ultraviolet, X-ray and gamma-ray astronomy started to develop, so that today, just 50 years after, the energy range available for the astronomical observations comprises some 12 decades in energy:

$$10^{-6} \text{ eV} < \epsilon < 10^{13} \text{ eV} \tag{1.5}$$

Fig. 1.2 shows the definition of different "energy windows" of the multi-wavelength astronomy.

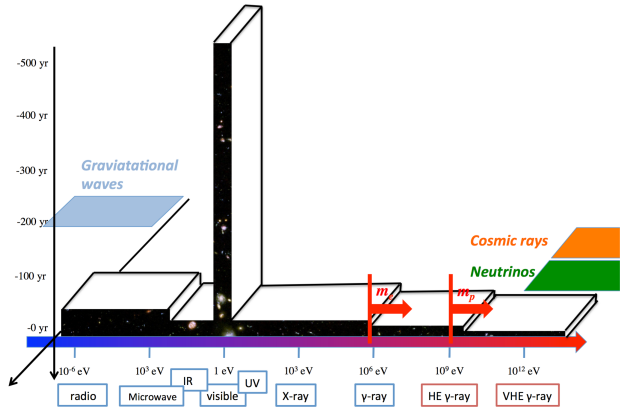


Figure 1.2: Timeline of the history of astronomy and definition of different energy / wavelength bands. and different astronomical "messenger" particles.

The tools of the multi-wavelength astronomy have opened a possibility of observing the effects of interactions of high-energy particles in astronomical sources. Photons with energies up to $10^{13}$ eV are produced by particles with energies at least $E > 10^{13}$ eV, i.e. much higher than the rest energies of proton and electron. These particles emit photons of different energies, from radio to $\gamma$-rays via a variety of emission mechanisms: synchrotorn, Compton scattering, Bremsstrahlung, pion production and decay. Combinaiton of multi-wavelength data is important for getting a complete picture of physical mechanisms of activity of the sources.

In a similar way, the high-energy sources also emit different types of particles, "astronomical messengers". Apart from photons, the most common "astronomical messenger" particles, information on mechanisms of operation of high-energy sources is also carried by neutrinos, cosmic rays and gravitational waves. Combinaiton of the "multi-messenger" data (Fig. 1.2) is equally important for understanding of the mechanisms of operation of sources.

In the context of the multi-wavelength astronomy, the term "High-Energy Astrophysics" is sometimes understood in a slightly different sense, than explained above. the term "High-Energy" might also refer to "photons energies higher than those of the visible / UV light". In this case the "High-Energy Astrophysics" research field comprises all possible sources and physical processes which manifest themselves through the X-ray and gamma-ray emission. This includes then not only processes

related to the presence of relativistic particles in the sources, but also thermal processes in astronomical objects with temperatures in the range above 100 eV (the low-energy boundary of the X-ray band).

## 1.1 Types of astronomical HE sources

Large part of astronomical sources emit radiation with thermal spectrum characterised by temperature $T$. The energies of particles generating this radiation could be estimated from the well-known relation

$$\langle E \rangle \sim \frac{3}{2} k_B T \tag{1.6}$$

where $k_B = 8.6 \times 10^{-5}$ eV K$^{-1}$ is the Boltzmann constant serving as a conversion coefficient between the units of temperature and energy units. Presence of relativistic particles in the thermal astronomical objects implies the temperature range

$$T \sim \frac{m_e c^2}{k_B} \simeq 0.6 \times 10^{10} \text{ K} \tag{1.7}$$

for the objects containing relativistic electrons or

$$T \sim \frac{m_p c^2}{k_B} \simeq 10^{13} \text{ K} \tag{1.8}$$

for the objects with high-energy protons.

The temperature range $T \sim 10^{10}$ K might be reached in the interiors of stars or at the final stage of life of massive stars when they explode as supernovae. The surface temperatures of the stars are typically much lower, not exceeding $10^5$ K, so that solar-like and massive stars powered by the nucleosynthesis reactions are not the sources of interest in the High-Energy Astrophysics domain.

Much higher temperatures are sometimes reached in the objects powered by the release of gravitational (rather than nuclear) energy. A typical first estimate of the temperature of a gravitationally collapsing matter is given by the virial theorem

$$T \sim \frac{2}{3} \frac{\langle E \rangle}{k_B} \sim \frac{1}{3} \frac{U}{k_B} \sim \frac{G_N M m_p}{3 k_B R} \tag{1.9}$$

where $G_N = 6.7 \times 10^{-8}$ cm$^3$/(g s$^2$) is the gravitational constant, $M, R$ are the mass and size of the collapsing matter configuration and $U$ is the gravitational potential energy. Typical particle energies become relativistic, $\langle E \rangle \sim m_p c^2$, if the body is compact enough, with the size

$$R \sim \frac{G_N M}{c^2}. \tag{1.10}$$

This size estimate is about the gravitational radius of a body with the mass $M$

$$R_{grav} = \frac{G_N M}{c^2} \simeq 1.5 \times 10^5 \left[ \frac{M}{M_\odot} \right] \text{ cm}. \tag{1.11}$$

Objects of the size comparable to the gravitational radius are called "compact objects". The known astronomical compact object classes are *neutron stars* and *black holes*, including the supermassive black holes in the centres of galaxies and stellar mass black holes.

These two classes of objects are powering most of the astronomical sources studied in High-Energy Astrophysics, including

- Active Galactic Nuclei (AGN):

  - Seyfert galaxies (Sy)
  - quasars / blazars (QSO)
  - radio galaxies
- X-ray binaries (XRB):
  - Low-mass X-ray binaries (LMXRB)
  - High-mass X-ray binaries (HMXRB)
  - Micorquasars
- end products of the life cycle of massive stars:
  - supernova remnants (SNR)
  - pulsars and pulsar wind nebulae (PWN)
  - gamma-ray bursts (GRB)

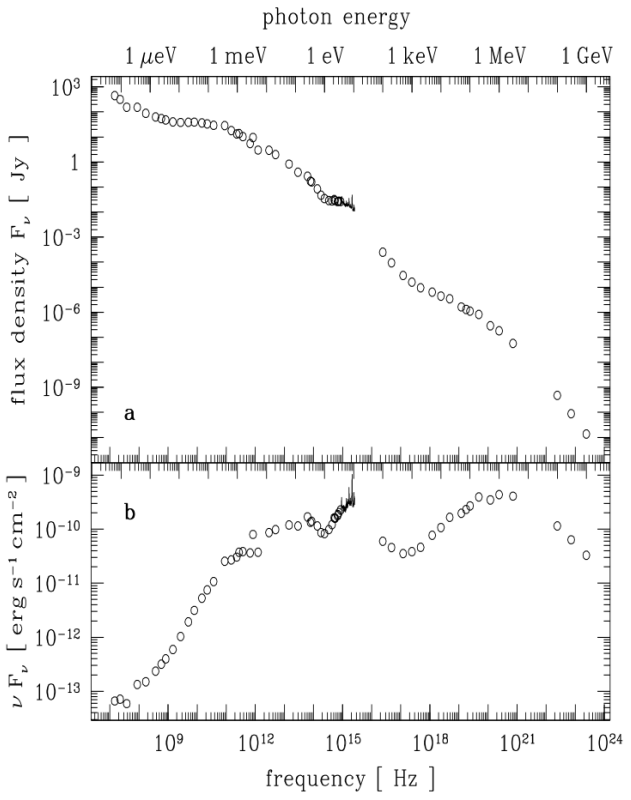


Figure 1.3: Spectral energy distribution of the quasar 3C 273, in two representations. The upper plot shore the differential flux, which is energy flux per unit energy or frequency. This flux is measured in the units of Jansky, 1 Jy= $10^{-23}$ erg/(cm$^2$ s Hz). The lower panel show the energy flux as a function of energy. From the Ref. [5].

Observations using the tools of multi-wavelength astronomy show that significant part of High-Energy Astrophysics sources does not emit radiation with thermal spectrum. Instead, they reveal signal which is spread over many decades of energy. Fig. 1.3 shows an example of such broad band spectrum in the quasar 3C 273. The broad range of photon energies is explained by the broad range of the energies of charged particles (electrons, protons) which have produced the photons. In the particular case of 3C 273, one could see that particle energies should be spread over several decades in energy.

## 1.2 Types of physical processes involved

High-energy particles with broad energy distribution usually loose their energy via various radiative energy loss channels, before being able to "thermalise" (i.e. to establish thermal distribution in momenta). The main radiative (ie. "accompanied by photon production") energy loss channels for electrons are

- synchrotron / curvature radiation,
- inverse Compton emission,
- Bremsstrahlung

A non-radiative energy loss especially important for mildly relativistic and non-relativistic electrons is

- Coulomb (ionisation) energy loss

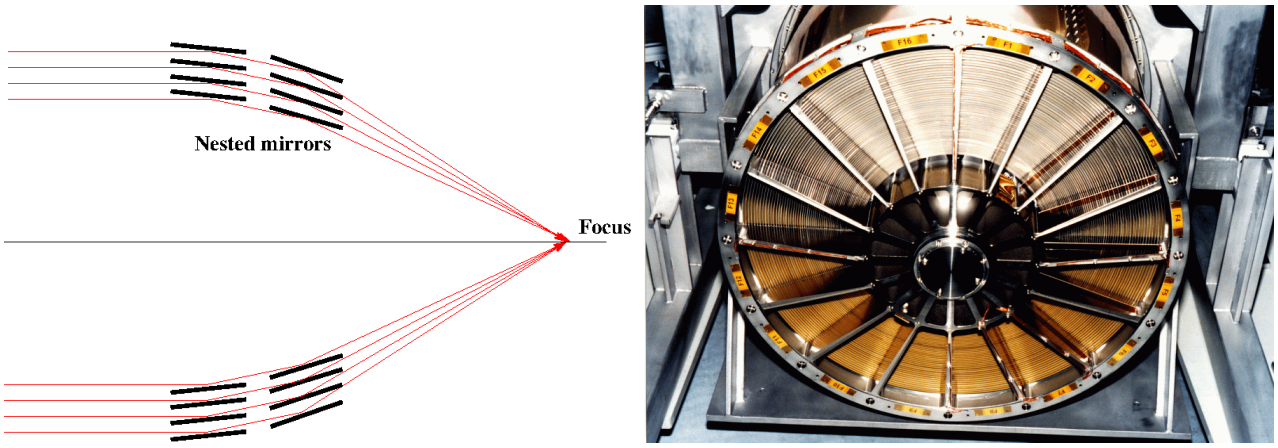


Figure 1.4: Left: the principle of grazing incidence optics used in X-ray telescopes. Right: the set of nested mirrors of the X-ray telescope *XMM-Newton*.

All these radiative and non-radiative channels contribute to larger or smaller extent to the formation of spectra of high-energy particles in the sources and to the formation of the broad-band emission spectra of the type shown in Fig. 1.3 for the quasar 3C 273.

In the case of high-energy protons the main radiative energy loss channel is

- production and decay of neutral and charged pions in interactions with matter and radiation fields.

The non-radiative Coulomb losses are also important for the lower energy mildly relativistic protons.

## 1.3 Observational tools

A complete understanding of the physics of sources with photon emission spectra extending from radio to gamma-rays (like 3C 273, shown in Fig. 1.3), is possible only with the detailed information on the imaging, spectral and timing information in all energy bands. This means that the observational tools of High-Energy Astrophysics include telescopes across all energy bands, including radio, infrared, visible, UV, X-ray and gamma-ray bands.

However, the term "experimental / observational High-Energy Astronomy" is usually reserved for telescopes and observational techniques in the X-ray and gamma-ray bands, with the visible / infrared astronomy and radio astronomies considered to be separate disciplines on their own.

X-rays and gamma-rays do not reach the ground. Observations in the X-ray and gamma-ray bands are, therefore, possible only with telescopes placed outside the Earth atmosphere in space. This explains why the age of High-Energy Astronomy has started only at the end of 1960th with the invent of the space flight.

Another peculiarity of the telescopes used in High-Energy Astronomy stems from the fact that, contrary to radio-infrared-visible radiation, X-ray and gamma-ray photons tend to interact with the telescope material in a destructive way, so that it is difficult to focus the signal with the conventional lenses / mirrors without destroying the photons. This is explained by the fact that the energy of each photon is comparable of higher than the ionisation energy of atoms composing the lens / mirror. As a result, the collisions of photons with atoms are inelastic and destructive.

This problem is partially overcome in the X-ray telescopes, where a special type of optical setup enables focusing of X-ray photons with energies up to 10 keV. The principle of the setup, known under the name of "grazing incidence optics", is shown in Fig. 1.4. To avoid the destructive interaction of X-rays with the lens / mirror material, the X-ray photons are falling on the mirror surfaces at large

incidence angles ("grazing" angles). A single grazing incidence focusing mirror (which could be e.g. segments of parabola) would have very small collection area, because it would intercept only a small faction of the X-ray photons. Stacks of nested mirror segments are used to achieve significant collection areas (in the range of $\sim 100 - 1000$ cm$^2$) with the grazing incidence technique. The right panel of Fig. 1.4 shows an example of the mirror of the X-ray telescope XMM-Newton, which is a European Space Agency (ESA) mission now in orbit.

Focusing photons of higher and higher energies would require the nested mirror systems with smaller and smaller grazing incidence angles. This, in turn, would imply larger and larger focal lengths. Thus, the grazing incidence technique stops to work at high energies (nowadays about 50 keV, achieved with the NASA X-ray telescope Nu-STAR). At higher energies astronomical observations are done without the use of focusing.

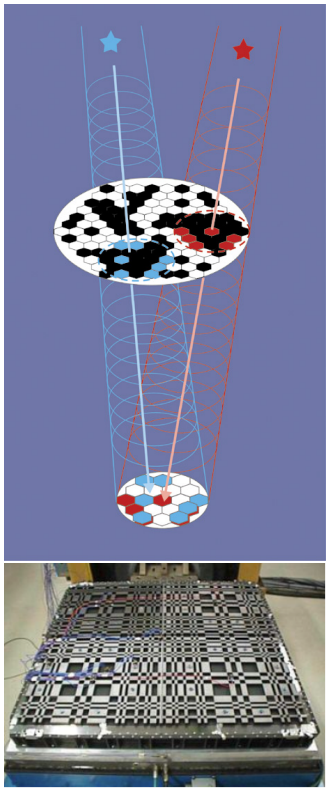

Figure 1.5: The principle of the coded mask optics and the coded mask of IBIS telescope on board of *INTEGRAL*.

One example of non-focusing optics is the "coded mask" technique, which is a direct development of the method of pinhole camera. This technique is illustrated in Fig. 1.5. Signal from an astronomical source passing through the mask (a plane with a set of holes) casts a particular shadow pattern on the detector plane. Registering this shadow pattern one could determine the source position on the sky via a straightforward ray tracing. Shadow patterns cast by different sources in the field of view overlap, but they are recognisable one-by-one, so that the ray tracing could be done for each source separately. This technique is used in a number of telescope currently operating in the hard X-ray / soft gamma-ray band, including the ESA INTergnational Gamma Ray Laboratory (INTEGRAL). The coded mask of the IBIS imager on board of INTEGRAL is shown in Fig. 1.5.

At the energies higher than $\sim 1$ MeV even the coded mask imaging would not work, because it would require a prohibitively heavy and thick mask which would be able to block gamma-rays. In this energy band telescopes do not use any imaging equipment at all. Instead, each gamma-ray is individually detected and it energy and arrival direction is determined. The observational data consist of the lists of gamma-rays detected from a given region of the sky in a given time span. Positions of sources of gamma-rays on the sky are identified by the clustering of large number of gamma-rays coming from particular directions. This principle of observations is used e.g. by the Fermi gamma-ray telescope operating in the 0.1-100 GeV energy band. Its setup is shown in Fig. 1.6. High-energy gamma-rays entering the telescope are converted into electron-positron pairs in one of the layers of the Tracker (the upper multi-layer part of the detector in Fig. 1.6). Trajectories of electron and positron are "tracked" by the Tracker and then energies of both particles are measured by the Calorimeter, which is the lower thicker layer of the detector shown in Fig. 1.6.

At the energies higher than $\sim 100$ GeV, the space-based detectors are unable to perform sensible astronomical observations, because of their limited collection area. In this energy band, each photon carries macroscopic energy (100 GeV=0.16 erg). The power of astronomical sources is carried by a small number of highly energetic photons and the overall number of photons rapidly decreases with the increase of the energy of each photon. Typical luminosities of astronomical sources are such that in the energy band above 100 GeV only about one or less photons per year could be detected by an instrument with collection area about 1 m$^2$.

Astronomical observations in the Very-High-Energy (VHE) band (photon energies above 100 GeV) are possible only with setups with extremely large collection areas (in the range of $10^4 - 10^6$ m$^2$). Such collection areas are provided by the ground-based Cherenkov telescope arrays, see Fig. 1.7.

The principle of detection of VHE gamma-rays is based on the fact that these gamma-rays produce electromagnetic cascades when they penetrate in the atmosphere. High-energy particles in the cascade move with the speed faster than the speed of light in the air and produce Cherenkov radiation in the UV wavelength range. Large optical reflectors are used to sample this Cherenkov light which appears for short periods of time (about ten nanoseconds) as bright "traces" of the gamma-ray induced cascade in the UV light. The information on the arrival direction and energy of the initial VHE gamma-ray is obtained via stereoscopic imaging of the cascade in the atmosphere (see Fig. 1.7, left panel). Right panel of Fig. 1.7 shows a 17 meter dish of the MAGIC telescope as an example of the large reflectors used by the Cherenkov telescopes.

## 1.4 Natural System of Units

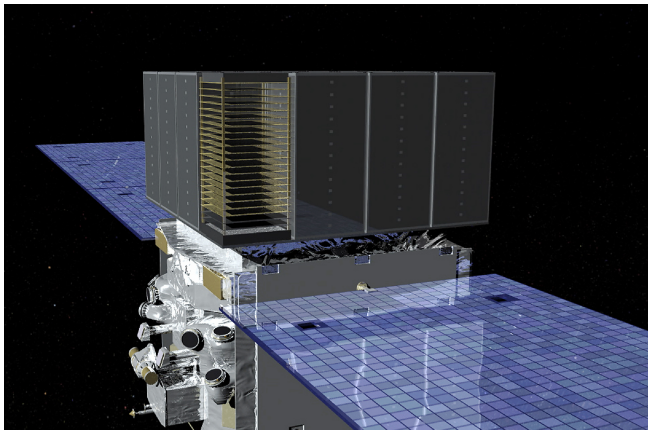

Figure 1.6: Fermi LAT telescope. The upper part of the telescope made of many layers is the Tracker. The lower thick layer part is Electromagnetic Calorimeter.

High-Energy Astrophysics subject relates particle physics and astronomy. These two branches of science use different unit conventions and it is sometimes challenging to convert the "language" of particle physicists into the "language" of astronomers and vice versa. A convenient approach is to reduce both astronomical and particle physics quantities and formulae to put them into a common unit system. Thoughout this course the common system of units will be the Natural System of Units, with the Gaussian version for electromagnetic quantities (as opposed to Heaviside-Lorentz, with quantities typically differing by $4\pi$ factors between Gaussian and Heaviside-Lorentz systems, see discussion in Ref. [6]).

The idea of the Natural system of units is to reduce the number of fundamental constants to the necessary minimum. This implies typically getting rid of the constants serving for unit conversions. For example, the Boltzman constant $k_B$ serves for conversion between the units of temperature (which is, in essence a measure of energy) and energy:

$$k_B = 8.6 \times 10{-}5 \text{ eV K}^{-1} = 1 \tag{1.12}$$

This means that in the Natural system of units the temperature is always measured in electronvolts, instead of Kelvins. Whenever a measurement is provided in Kelvins, one immediately converts it into electronvolts using the relation

$$1 \text{ K} = 8.6 \times 10^{-5} \text{ eV} \tag{1.13}$$

The same is done with the electric and magnetic permeabilities of vacuum, encountered in the International System of Units:

$$4\pi\epsilon_0 = 4\pi\mu_0 = 1 \tag{1.14}$$

which serve for the introduction of the charge units (Coulomb) in this system.

In a similar way, one could see that the speed of light is, in a sense, a constant for conversion of the units of time and distance: one could measure distance in time units, with the unity the distance travelled by photons in one second, or, vice versa, once could measure time in the distance units, with the unity being time in which photon crosses the distance of 1 cm. Thus, imposing

$$c = 3 \times 10^{10} \text{ cm/s} = 1 \tag{1.15}$$

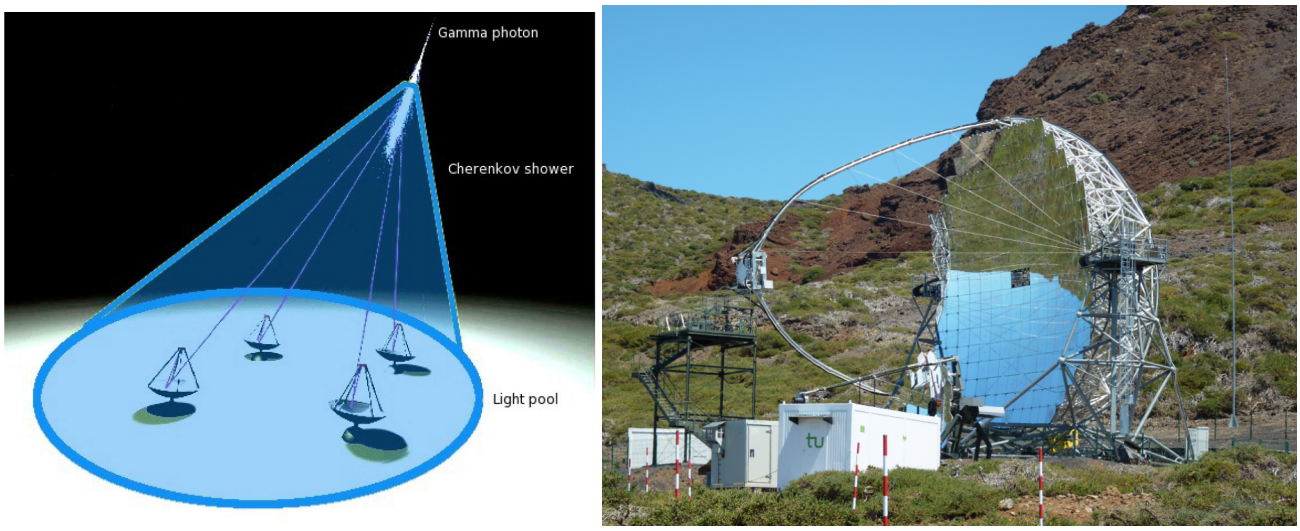


Figure 1.7: Left: the principle of operation of Cherenkov telescopes. RIght: one of the two Cherenkov telescopes of MAGIC stereo pair.

one obtains a conversion between different time-distance units:

$$1 \text{ s} = 3 \times 10^{10} \text{ cm} \tag{1.16}$$

The speed of light serves also for conversion of the units of mass into the units of energy via the relation $E = mc^2$. Thus, any measurement of the mass in grams could be converted into ergs or electronvolts.

The Planck constant relates the energy and frequency of the photon: $E = \hbar\omega$. Setting

$$\hbar = 6.6 \times 10^{-16} \text{ eV s} = 1 \tag{1.17}$$

one obtains a way of measurement of energy in the units of frequency (or inverse time) and vice versa:

$$1 \text{ eV} = 1.5 \times 10^{15} \text{ s}^{-1} \tag{1.18}$$

(notice that the frequency of photons given in the astronomical measurements is usually $\nu = \omega/(2\pi)$, so that the conversion between Hz (frequency of radiation) and eV (energy of photons) differs from the above relation by a $2\pi$ factor.

Combining the conversion of centimetres into seconds and seconds into elevtronvolts one finds a relation

$$\hbar c = 2 \times 10^{-5} \text{ eV cm} = 1, \quad \rightarrow \quad 1 \text{ eV} = 5 \times 10^{4} \text{ cm}^{-1} \tag{1.19}$$

In the Natural System of units the electric charge is dimensionless. This is clear from the expression for the fine structure constant:

$$\alpha = \frac{1}{137} = \frac{e^2}{4\pi\epsilon_0\hbar c} = e^2 \tag{1.20}$$

The numerical value of the electron charge is

$$e = \sqrt{\alpha} \simeq 0.085 \tag{1.21}$$

Magnetic field is measured in the units of [energy]$^2$, as it is clear from the expression for the energy density of magnetic field

$$U = \frac{\mu_0 B^2}{2} = \frac{B^2}{8\pi} \tag{1.22}$$

The energy density is the quantity measured in e.g. [eV/cm$^3$]. Since $cm^{-1}$ is also an energy unit, the units of $U$ are also [eV$^4$]. To match the dimensions in the right and left hand side of the above equation, $B$ should be measured in the units of [eV$^2$]. The conversion between Gauss (the units of magnetic field in the CGS system) and eV$^2$ could be found from the relation

$$U_B = \frac{[B/1\ \mathrm{G}]^2}{8\pi}\frac{\mathrm{erg}}{\mathrm{cm}^3} \tag{1.23}$$

Taking into account the conversion between the energy units ergs and eV

$$1\ \mathrm{eV} = 1.6 \times 10^{-12}\ \mathrm{erg} \tag{1.24}$$

one finds

$$1\ \mathrm{G} \simeq 0.07\ \mathrm{eV}^2 \tag{1.25}$$

The conversion between Tesla (magnetic field units in the International System) and Gauss is

$$1\ \mathrm{T} = 10^4\ \mathrm{G} \tag{1.26}$$

Combining the last and before-last equations one gets a conversion between Tesla and eV$^2$.

Other useful conversion coefficients which are needed to bring the astronomical and particle physics data to the common system of units are

- energy/power

$$\begin{aligned} 1\ \mathrm{J} &= 10^7\ \mathrm{erg} = 6.25 \times 10^{18}\ \mathrm{eV} \\ 1\ \mathrm{Jy} &= 10^{-23}\ \mathrm{erg}/(\mathrm{cm}^2\ \mathrm{s\ Hz}) \end{aligned} \tag{1.27}$$

- distance

$$\begin{aligned} 1\ \mathrm{pc} &= 3 \times 10^{18}\ \mathrm{cm} \\ 1\ \mathrm{AU} &= 1.5 \times 10^{13}\ \mathrm{cm} \\ 1\ \text{Å} &= 10^{-8}\ \mathrm{cm} \end{aligned} \tag{1.28}$$

- mass / energy

$$\begin{aligned} 1M_\odot &= 2 \times 10^{33}\ \mathrm{g} \simeq 1.8 \times 10^{54}\ \mathrm{erg} \simeq 10^{66}\ \mathrm{eV} \\ m_e &= 0.9 \times 10^{-27}\ \mathrm{g} = 5 \times 10^5\ \mathrm{eV} \\ m_p &= 1.7 \times 10^{-24}\ \mathrm{g} = 0.94 \times 10^9\ \mathrm{eV} \end{aligned} \tag{1.29}$$

- cross section

$$1\ \mathrm{barn} = 10^{-24}\ \mathrm{cm}^2 \tag{1.30}$$

This set of conversion formulae will be systematically used in numerous numerical estimates encountered in the following chapters.

One important note concerns the gravitational force and Newton constant. From the expression of the Newton's law

$$ma = \frac{G_N M m}{r^2} \tag{1.31}$$

it is clear that the dimensionality of the Newton constant is [mass]$^{-2}$ or, equivalently, [length]$^2$. This means that it is not possible to set this constant to one in the Natural System of units. Instead, the numerical value of the Newton constant is

$$G_N = 6.7 \times 10^{-8}\frac{\mathrm{cm}^3}{\mathrm{g\ s}^2} = \frac{1}{(10^{19}\ \mathrm{GeV})^2} = \frac{1}{M_{Pl}^2} \tag{1.32}$$

The energy (or mass) scale entering the Newoton's constant is called the Planck scale.

## 1.5 Excercises

**Excercise 1.1.** Estimate the temperature of supernova remnant shell assuming that the kinetic energy of explosion ($10^{51}$ erg) is ultimately "thermalized" within the supernova shell of total mass $1M_{\odot}$.

**Excercise 1.2.** Estimate the temperature of interstellar medium around a star forming region of 100 pc size in which 100 supernovae have exploded on short time scale.

**Excercise 1.3.** Find the temperature of a black body of mass about $M_{\odot}$ and radius about 10 km (neutron star) and 1000 km (white dwarf) emitting radiation at Eddington limit $L = 10^{38}$ erg/s.

**Excercise 1.4.** Using the Natural System of Units, find the mass $M$ of a "quantum black hole", a body for which its gravitational radius $R_g = G_N M$ equals its "Compton-like" wavelength, $\lambda = 1/M$.

**Excercise 1.5.** Using the Natural System of Units, find the strength of "QED-scale" magnetic field $B$ for which motion of mildly relativistic (velocity $v \sim 1$) charged particles of mass $m$ and charge $e$ has to be described in quantum mechanics framework. This happens when the gyroradius $R_L = m/(eB)$ becomes equal to the "Compton-like" wavelength, $\lambda = 1/m$.

# Chapter 2

# Radiative Processes

## 2.1 Radiation from a moving charge

Most of the formulae in this chapter for the radiative processes involving electrons (synchrotron and curvature radiation, Compton scattering and Bremmstrahlung emission) are different applications of the basic formulae for the dipole radiation of an accelerated charge. Taking this into account, this section reminds the derivation of the accelerated charge radiation.

Electromagnetic field is a solution of Maxwell equations [7]

$$\frac{\partial F^{\mu\nu}}{\partial x^{\nu}} = -4\pi j^{\mu}. \tag{2.1}$$

where $x^{\mu} = (t, \vec{x})$ are the four-coordinates and $j^{\mu}$ is the four-current. Expressing the electromagnetic field tensor through the 4-potential $F_{\mu\nu} = \partial_{\mu}A_{\nu} - \partial_{\nu}A_{\mu}$, we rewrite the Maxwell equations for the potential in the Lorentz gauge $\partial A^{\mu}/\partial x^{\mu} = 0$ in the form of inhomogeneous wave equation

$$\frac{\partial^2 A^{\mu}}{\partial x_{\nu}\partial x^{\nu}} = 4\pi j^{\mu} \tag{2.2}$$

We are interested in the particular case of a point charge $e$ moving along a trajectory $\vec{r} = \vec{r}_0(t)$. Such a charge creates the 4-current $j^{\mu} = e(\delta(\vec{r} - \vec{r}_0(t)), \vec{v}\delta(\vec{r} - \vec{r}_0(t)))$ where $\vec{v} = d\vec{r}_0/dt$ is the velocity. Solution of the wave equation in a point $\vec{r}$ at the moment of time $t$ is determined by the state of motion of the charge at the moment of time $t'$ implicitly found from the relation

$$t' + \left|\vec{r} - \vec{r}_0(t')\right| = t \tag{2.3}$$

The solution of the system of wave equations for the potential is known to be the Lienard-Wichert potential $A_{\mu} = (\phi, \vec{A})$

$$\phi(r,t) = \left.\frac{e}{(R - \vec{v}\cdot\vec{R})}\right|_{t'}, \quad \vec{A}(r,t) = \left.\frac{e\vec{v}}{(R - \vec{v}\cdot\vec{R})}\right|_{t'}, \tag{2.4}$$

where $\vec{R} = \vec{r} - \vec{r}_0$. Electric and magnetic fields corresponding to this potential could be calculated from relations $\vec{E} = \partial\vec{A}/\partial t - \partial\phi/\partial\vec{x}$, $\vec{B} = (\partial/\partial\vec{x}) \times \vec{A}$. This gives an expression

$$\begin{aligned} \vec{E} &= \frac{e(1-v^2)}{(R - \vec{v}\cdot\vec{R})^3}(\vec{R} - R\vec{v}) + \frac{e}{(R - \vec{v}\cdot\vec{R})^3}\left[\vec{R} \times \left[(\vec{R} - R\vec{v}) \times \frac{d\vec{v}}{dt}\right]\right] \\ \vec{B} &= \frac{1}{R}\left[\vec{R} \times \vec{E}\right] \end{aligned} \tag{2.5}$$

If the velocity of the charge does not change in time, $dv/dt = 0$, the second term is absent and the first term just gives the Coulomb field of the charge, falling as $R^{-2}$ at large distances. Using the rules of Lorentz transformation of electromagnetic tensor, one finds that in this case the magnetic field is absent in the reference system comoving with the charge.

Accelerated motion of the charge $dv/dt \neq 0$ leads to the appearance of an additional term which falls as $1/R$ at large distances. Both electric and magnetic field due to this term are orthogonal to the direction toward the charge. This is the field of electromagnetic wave generated by the accelerated motion. A qualitative understanding of the appearance of electromagnetic wave could be obtained via a simple geometrical calculation, see e.g. [2, 1].

At large distances from the source, $r \gg r_0$, and for non-relativistic charge motion, $v \ll 1$, one could approximate $R \simeq r$. In this case the second term in the expression from the electric field of slowly moving charge could be rewritten in the form

$$\vec{E} \simeq \frac{1}{r}\left[\left[\ddot{\vec{d}} \times \vec{n}\right] \times \vec{n}\right] \tag{2.6}$$

where the dipole moment $\vec{d} = e\vec{r}_0$ and the unit vector $\vec{n} = (\vec{r})/r$ are introduced. The magnetic field in these notations is

$$B \simeq \frac{1}{r}\left[\ddot{\vec{d}} \times \vec{n}\right] \tag{2.7}$$

Both electric and magnetic fields are orthogonal to the direction from the charge to the observation point $\vec{n}$ and they are also orthogonal to each other. Such configuration is typical for the electromagnetic wave propagating in the direction $\vec{n}$. The energy flux carried by the wave is given by the Poynting vector

$$\vec{S} = \frac{\left[\vec{E} \times \vec{B}\right]}{4\pi} = \frac{B^2}{4\pi}\vec{n} \tag{2.8}$$

Substituting the expression for $B$ one finds the flux $dI$ in the solid angle $d\Omega$ in the direction $n$ at an angle $\theta$ with respect to the direction of $\ddot{\vec{d}}$

$$\frac{dI}{d\Omega} = (\vec{S} \cdot \vec{n}) = \frac{\ddot{d}^2}{4\pi}\sin^2\theta \tag{2.9}$$

One could see that the intensity of emission is directed in a broad angular range preferentially in the direction orthogonal to the acceleration $\ddot{\vec{d}}$.

Integration of the above expression over $0 < \theta < \pi$ gives ($d\Omega = 2\pi \sin\theta d\theta$)

$$I = \frac{2\ddot{d}^2}{3}. \tag{2.10}$$

This is the Larmor formula for the intensity of dipole radiation by an accelerated charge.

This total power is emitted in the form of photons of different energies. To know the energy distribution, or spectrum, of the radiation we decompose the overall power onto power at a given frequency $\omega$ by doing the Fouriver transform. For this we use the formula of Fourier analysis stating that $\int_{-\infty}^{\infty} |f(t)|^2 dt = 4\pi \int_{-\infty}^{\infty} |f(\omega)|^2 d\omega$. This means that in the non-relativistic motion case

$$\int_{-\infty}^{\infty} \frac{dI}{d\Omega} dt = \int_{-\infty}^{\infty} \frac{|\ddot{d}|^2}{4\pi}\sin^2\theta dt = \int_{-\infty}^{\infty} \omega^4 |\hat{d}(\omega)|^2 \sin^2\theta d\omega = \int_{-\infty}^{\infty} \frac{d\hat{I}(\omega)}{d\Omega} d\omega \tag{2.11}$$

and the spectral energy density of radiation at the frequency $\omega$ is

$$\frac{d\hat{I}(\omega)}{d\Omega} = \omega^4 |\hat{d}(\omega)|^2 \sin^2\theta \tag{2.12}$$

Here the hat denotes the Fourier transform of the function, e.g.

$$d(t) = \int_{-\infty}^{\infty} e^{-i\omega t}\hat{d}(\omega)d\omega \tag{2.13}$$

For a relativistic charge, one introduces the 4-velocity $u^\mu = dx^\mu/d\tau$ where $\tau$ is the proper time along the particle trajectory, and the 4-acceleration $a^\mu = du^\mu/d\tau = (d\gamma/d\tau, d(\gamma\vec{v})/d\tau)$, with $\gamma = 1/\sqrt{1-v^2}$ being the particle gamma factor. The Larmor formula rewritten in the 4-vector notations reads

$$I = \frac{2e^2}{3}a_\mu a^\mu = \frac{2}{3}e^2\left(\left(-\frac{d\gamma}{d\tau}\right)^2 + \left(\frac{d(\gamma\vec{v})}{d\tau}\right)^2\right) \tag{2.14}$$

Expressing the derivative of $\gamma$ through the derivative of $v$ and substituting $dt/d\tau = \gamma$ one could rewrite the last formula in the form

$$I = \frac{2}{3}e^2\gamma^6\left((\vec{v}\cdot\dot{\vec{v}})^2 + \frac{1}{\gamma^2}(\dot{\vec{v}})^2\right) \tag{2.15}$$

where dot denotes the coordinate time derivative $d/dt$. The quantity $(\vec{v}\cdot\dot{\vec{v}}) = va_{||}$ is the component of particle acceleration parallel to the velocity. One could introduce also the normal component of the acceleration via relation $\dot{\vec{v}}^2 = a_{||}^2 + a_\perp^2$, so that the Larmor formula becomes

$$I = \frac{2}{3}e^2\gamma^6\left(a_{||}^2 + \frac{1}{\gamma^2}a_\perp^2\right) \tag{2.16}$$

## 2.2 Curvature radiation

Let us consider a relativistic particle with gamma factor $\gamma$ moving along a circle of the radius $R$ with the speed $v$. The angular frequency of such motion is $\omega_0 = v/R$. The only component of acceleration different from zero is $a_\perp = \omega_0 v$. The Larmor formula (2.16) gives the total power of emission (which is minus particle energy loss rate)

$$I = \frac{2}{3}e^2\gamma^4\omega_0 v^2 = \frac{2}{3}\frac{e^2\gamma^4 v^4}{R^2} \tag{2.17}$$

The spectrum of emission from a non-relativistic particle in a circular orbit could be found in a straightforward way. The velocity and acceleration are varying periodically with the period $T = 2\pi/\omega_0$, so that the only non-zero component of the Fourier transform of $d(t)$ is $\hat{d}(\omega_0)$. This means that the emission spectrum (for the non-relativistic motion case) is sharply peaked at the frequency $\omega_0$.

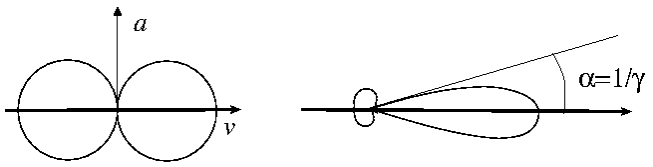


Figure 2.1: Angular pattern of dipole emission from non relativistic (left) and relativistic (right) particles.

The second time derivative of the dipole moment is a vector rotating in the plane of the circular motion of the particle. The angular distribution of the emitted dipole radiation is given by Eq. (2.9) and is shown in the left panel of Fig. 2.1.

In the relativistic case, the angular distribution pattern changes due to the Doppler boosting. To find the characteristic boosting pattern, consider a particle moving along axis $x$ with the speed $v$ close to the speed of light, $v \sim 1$. In the reference system comoving with the particle, particle motion is non-relativistic and emission (e.g. dipole radiation described above) is in a broad range of angles. The transformation to the comoving reference frame has the form

$$x' = \gamma(x - vt); \quad y' = y, \quad z' = z, \quad t' = \gamma(t - vx). \tag{2.18}$$

Transformation of velocities between the laboratory and comoving frame is

$$u_x = \frac{u'_x + v}{1 - vu'_x}, \quad u_y = \frac{u'_y}{\gamma(1 + vu'_x)}, \quad u_z = \frac{u'_z}{\gamma(1 + vu'_x)}. \tag{2.19}$$

Consider a photon which is emitted in the direction normal to the particle motion along $y$ axis in the comoving frame, $u'_x = u'_z = 0$. In the laboratory frame the components of photon velocity are

$$u_x = v, \quad u_y = \frac{u'_y}{\gamma}, \quad u_z = 0 \tag{2.20}$$

The angle between the direction of motion of photon and particle velocity in the laboratory frame is, therefore,

$$\alpha = \frac{u_y}{u_x} = \frac{1}{v\gamma} \simeq \frac{1}{\gamma} \tag{2.21}$$

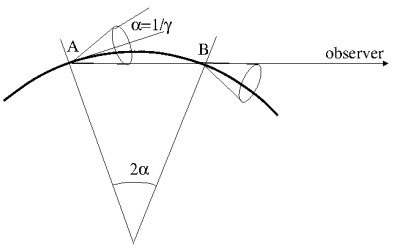


Figure 2.2: Geometry of emission by relativistic particle in circular motion.

A similar estimate, $\alpha \sim \gamma^{-1}$ could be found for the broad range of photon directions in the comoving frame, which are not almost aligned with the direction of particle velocity. Thus, the effect of the Doppler boosting on any broad angle radiation pattern is to compress this pattern into a narrow range of directions $\alpha \lesssim \gamma^{-1}$ around the direction of particle velocity $v$.

Relativistic beaming also dramatically changes the spectrum of radiation. Consider an observer situated in the plane of circular motion at large distance from the particle. (S)he detects the radiation in the form of short pulses, each time when the beam with an opening angle $\alpha \simeq \gamma^{-1}$ directed along particle velocity passes through the line of sight. The duration of the pulse could be readily calculated from geometry shown in Fig. 2.2. The radiation is visible from a fraction of the circle of particle trajectory spanning an angle $2\alpha$. The length of the arc of the angular size $2\alpha$ is $L = 2\alpha R$ and the time interval during which particle emits in the direction of observer is therefore $\Delta t = 2\alpha R/v$. Suppose that the particle passes the point A at the moment $t_0$. The photon emitted at this point arrives at the location of observer after a time delay $\delta t_A = d/c$, where $d$ is the distance to the observer. The last photon in the direction of the observer is emitted at the point B, at the moment $t_A = t_0 + \Delta t$. It arrives at the location of the observer at the moment $t_B = t_0 + \Delta t + \delta t_B$, where $\delta t_B = (d - L)/c$. The overall duration of the pulse seen by the observer is

$$\Delta t_{obs} = t_B - t_A = \Delta t + \delta t_B - \delta t_A = \Delta t\,(1 - v) = \frac{2R}{\gamma v}(1 - v) = \frac{2R}{\gamma^3 v(1 + v)} \simeq \frac{R}{\gamma^3} \tag{2.22}$$

where we have substituted $v \simeq 1$ in the last equality. The Fourier transform of the time sequence of pulses detected by the observer has all harmonics up to the frequency

$$\omega_{curv} \sim \frac{1}{\Delta t_{obs}} \sim \frac{\gamma^3}{R} \tag{2.23}$$

It is useful to have a numeric reference value for this frequency for the future estimates:

$$\epsilon_{curv} = \hbar\omega_{curv} = \frac{\hbar c\gamma^3}{R} \simeq 2 \times 10^4 \left[\frac{\gamma}{10^5}\right]^3 \left[\frac{R}{10^6\ \mathrm{cm}}\right]^{-1}\ \mathrm{eV} \tag{2.24}$$

One could understand the above formula in the following way. Relativistic electrons with energies $E_e = \gamma m_e \simeq 100$ GeV confined within a region of the size $R \sim 10$ km, they inevitably emit curvature radiation in the hard X-ray band, at the energies about $\epsilon_{curv} \sim 20$ keV. As an "everyday life" example

of such situation one could mention the past times when the LHC accelerator machine in CERN was still electron-positron collider LEP (Large Electron Positron). It was operating at the energies $E \sim 100$ GeV accelerated in the LHC tunnel of the radius $R \sim 10$ km. From Eq. (2.24) one could find that the electron beam was a source of hard X-rays.

Situation when high-energy particles are confined within an astronomical source of finite size is typical. Thus, generically, all astronomical sources hosting high-energy particle accelerators should be visible in telescopes, because the charged high-energy particles confined within the source emit (at least!) curvature radiation photons.

Particles emitting curvature radiation loose energy at the rate

$$-\frac{dE_e}{dt} = I \simeq \frac{2}{3}\frac{e^2\gamma^4}{R^2} \simeq 4 \times 10^{11} \left[\frac{\gamma}{10^5}\right]^4 \left[\frac{R}{10^6 \text{ cm}}\right]^{-2} \frac{\text{eV}}{\text{s}} \tag{2.25}$$

(see Eq. (2.17)). Once injected in such a compact region of space, TeV electrons loose all their energy within the time interval shorter than one second. Coming back to the LEP example, one could conclude from Eq. (2.25) that supporting the beam of accelerated electrons in the LEP accelerator machine required continuous "re-acceleration" of the beam. All the beam energy was continuously dissipated into the hard X-rays.

### 2.2.1 Astrophysical example (pulsar magnetosphere)

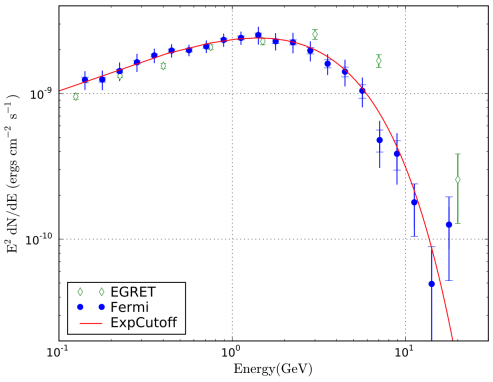


Figure 2.3: Spectrum of pulsed $\gamma$-ray emission from Vela pulsar (the brightest GeV $\gamma$-ray point source on the sky). From Ref. [8].

The reference example illustrating curvature radiation in astrophysical environments is the currently most often considered model of $\gamma$-ray emission from magnetospheres of pulsars.

Pulsars are strongly magnetised and fast spinning neutron stars, i.e. compact stars of the size $R_{NS} \sim 10^6$ cm, rotating at frequencies $1 - 10^3$ Hz and possessing magnetic fields in the range of $B \sim 10^{12}$ G. Most of the isolated point sources of GeV $\gamma$-rays in the Galactic Plane are pulsars. Spectrum of emission from the brightest pulsar on the sky, the Vela pulsar, is shown in Fig. 2.3.

The bright GeV $\gamma$-ray emission from the pulsars is pulsed at the period of rotation of the neutron stars ($1 - 10^3$ Hz). This implies that the $\gamma$-ray photons are produced close to the neutron star, in a region reasonably close to the surface of the neutron star. We adopt a first estimate $R \sim R_{NS} \sim 10^6$ cm and leave further details for the dedicated section on pulsars. This emission is detected at the energies exceeding 1 GeV. It is inevitably produced by relativistic particles.

As it is mentioned above, relativistic particles confined to a compact spatial region inevitably loose energy at least onto curvature radiation (there might be competing energy loss channels, we will consider them later on). Using Eq. (2.24) one could estimate the energies of electrons responsible for the observed $\gamma$-ray emission, under the assumption that the $\gamma$-rays are produced via curvature mechanism

$$E_e \simeq 2 \times 10^{12} \left[\frac{\epsilon_{curv}}{1 \text{ GeV}}\right]^{1/3} \left[\frac{R}{R_{NS}}\right]^{1/3} \text{ eV} \tag{2.26}$$

Assumption that emission observed in pulsars comes from the curvature radiation process provides, in a sense an upper bound on the energies of particles contained in the sources. Indeed, we will see later on in the course that most of the radiation processes encountered in High-Energy Astrophysics

are different variations of one and the same process of dipole radiation. Each time when trajectories of relativistic particles are deflected by some force, they start to radiate. The slowest possible deflection rate and, respectively, the largest possible extent of particle trajectory is when particle is deviated only when it crosses the entire astronomical source where it is confined. The slowest possible deflection rate leads to the "minimal" energy loss rate and to the emission of lowest energy photons. This is the case of curvature radiation with $R \; R_{NS}$ in pulsars. From these arguments one could conclude that typical energies of electrons confined around pulsars are

$$E_{e,\; pulsars} \lesssim 10^{12} \text{ eV} \tag{2.27}$$

This conclusion just stems from an observational fact that most of the pulsars have high-energy cut-offs in the spectra in the GeV energy band. It does not depend on the details of the model of particle acceleration and interactions which lead to the observed $\gamma$-ray emission.

## 2.3 Evolution of particle distribution with account of radiative energy loss

A competition between acceleration, energy loss and escape processes leads to formation of broad energy distribution of high-energy particles inside astronomical sources

$$\frac{dN_e}{dE} = f_e(E). \tag{2.28}$$

The index $e$ is introduced to distinguish the distribution of charged high-energy particles, e.g. electrons, from the distribution of photons emitted by these particles, which we will denote as $dN_\gamma/dE$.

The acceleration process injects particles of energy $E$ with a rate $Q_e(E)$. Then particles are cooling due to radiative and non-radiative losses, with a rate $\dot{E}$, which is also a function of energy. As a result, their energy decreases and $f_e(E)$ at the injection energy decreases, while $f_e(E - \int \dot{E} dt)$ increases. Particles do not disappear once injected, so that the function $f_e(E)$ should satisfy a continuity equation in the energy space

$$\frac{\partial f_e}{\partial t} + \frac{\partial}{\partial E}\left(\dot{E} f_e(E)\right) = Q_e(E,t) \tag{2.29}$$

The sense of this equation is that the increase / decrease of $f_e$ in a unit time in a given energy bin of the width $\Delta E$ at reference energy $E$ is given by the rate of injection $Q_e \Delta E$, by the rate influx of particles from the adjacent higher energy bin, $-\dot{E} f(E)\Big|_{E+\Delta E}$ and the rate of outflow into the adjacent lower energy bin $-\dot{E} f(E)\Big|_E$ ($\dot{E} < 0$ is "velocity" along the energy axis, compare with the continuity equation of the fluid dynamics: $\partial f/\partial t + \vec{\nabla}(f\vec{v}) = Q$ ).

In the above equation, $Q$ is a source of particles, but could also be the "leakage" of particles (then it is negative). The leakage, or escape of particles is often characterised by typical escape time $\tau_{esc}$, which could be a function of energy. Then, the source / leakage term, from dimensional reasons, has the form

$$Q_{e,esc} = \frac{f_e}{\tau_{esc}(E)} \tag{2.30}$$

so that the Eq. (2.29)

$$\frac{\partial f_e}{\partial t} + \frac{\partial}{\partial E}\left(\dot{E} f_e(E)\right) = Q_e(E,t) - \frac{f_e}{\tau_{esc}} \tag{2.31}$$

In the steady state situation, $\partial f/\partial t = 0$, in the absence of escape $\tau_{esc} \to \infty$, the solution of the above equation has the form

$$f_e(E) = \frac{1}{\dot{E}} \int_E^\infty dE' \; Q_e(E') \tag{2.32}$$

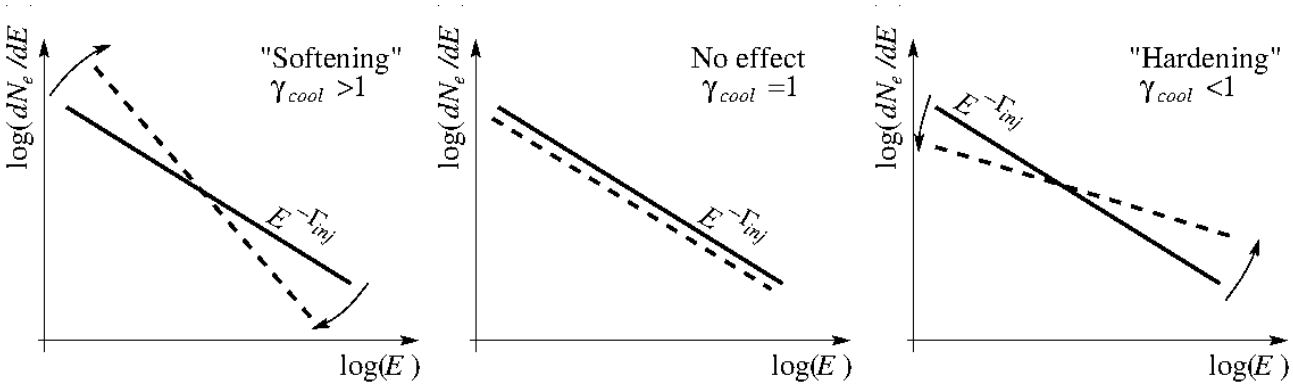


Figure 2.4: The effect of cooling on particle spectrum for different energy dependance of the cooling rate.

As an example, let us calculate the energy distribution of particles reached in the situation where the injection is a delta-function in energy $Q(E) \sim \delta(E - E_0)$. In this case the above solution of the equation takes the form

$$f_e(E) = \begin{cases} 1/\dot{E}, & E < E_0 \\ 0, & E > E_0 \end{cases} \tag{2.33}$$

If the cooling is provided by the curvature radiation, then $\dot{E} \sim E^4$ and

$$f_e(E) = \begin{cases} AE^{-4}, & E < E_0 \\ 0, & E > E_0 \end{cases} \tag{2.34}$$

where $A$ is a normalisation factor. One could see that cooling leads to a "pile up" of particles at lower energies: the number of particles per unit energy interval (or per decade in energy) increases with the decrease of their energy.

In general, if the energy loss rate scales with particle energy as $\dot{E} \propto E^{\gamma_{cool}}$, the effect of cooling on a powerlaw distribution of particles is "softening" or "hardening" of the spectrum, see Fig. 2.4.

## 2.4 Spectrum of emission from a broad-band distribution of particles

One could see from the previous subsection that typically high-energy particles are distributed over a wide energy range (e.g. form a powerlaw type spectra), rather than concentrate around a particular energy. Broad distribution of energies of emitting particles leads to a broad distribution of energies of emitted photons.

In general, the spectrum of emission from a distribution of electrons (protons) $dN_e/dE = f_e(E_e) \sim E_e^{-\Gamma_e}$ could be calculated once the spectrum of emission from mono energetic electrons $\Phi(E_e, E_\gamma)$ is known. The intensity $\Phi$ of emission at the energy $E_\gamma$ depends on the electron energy $E_e$. The emission from the distribution of electrons is given by the integral

$$\phi(E_\gamma) = \int \frac{dN_e}{dE_e} \Phi(E_e, E_\gamma) dE_e \tag{2.35}$$

Let us calculate the spectrum of curvature emission from a powerlaw distribution of electrons $dN_e/dE = f_e(E_e) \sim E_e^{-\Gamma_e}$ in the particular case of curvature radiation. Electrons of the energy $E_e$ emit curvature photons of the energy given by Eq. (2.24), $E_{\gamma,*} \sim E_e^3$. In the first approximation one could adopt a "delta-function approximation" for the spectrum of emitted photons, $\Phi(E_e, E_\gamma) \sim$

$\delta(E_\gamma - E_{\gamma,*})$. The normalisation of the emission spectrum is proportional to the rate of emission of photons , given by Eq. (2.25), the emission power, divided by the photon energy $E_\gamma = E_e^3/(m_e^3 R)$.

$$\Phi(E_e, E_\gamma) = \frac{E_e}{m_e R}\delta\left(E_\gamma - \frac{E_e^3}{m_e^3 R}\right) \tag{2.36}$$

Substituting this expression into (2.35) and taking the integral, we find

$$\begin{aligned}
\phi(E_\gamma) &\sim \int E_e^{-\Gamma_e}\frac{E_e}{m_e R}\delta\left(E_\gamma - \frac{E_e^3}{m_e^3 R}\right) dE_e \\
&\sim \int \frac{E_e^{1-\Gamma_e}}{m_e R}\frac{m_e^3 R}{3E_e^2}\delta\left(E_\gamma - \frac{E_e^3}{m_e^3 R}\right) d\left(\frac{E_e^3}{m_e^3 R}\right) \\
&\sim E_e^{-\Gamma_e - 1} \sim E_\gamma^{\frac{-\Gamma_e - 1}{3}}
\end{aligned} \tag{2.37}$$

Thus, the spectrum of emission from a power law distribution of emitting particles is also a power law.

We can generalise the above formula for an arbitrary dependence of the power of emission on the electron energy, $P(E_e) \sim E_e^{\gamma_{cool}}$ ($\gamma_{cool} = 4$ in the case of curvature radiation) and an arbitrary relation between photon and electron energy, $E_{\gamma,*} \sim E_e^\sigma$, ($\sigma = 3$ in the case of curvature emission). This gives

$$\phi(E_\gamma) \sim E_\gamma^{\frac{\gamma_{cool} + 1 - \Gamma_e - 2\sigma}{\sigma}} \tag{2.38}$$

We will reuse this formula to calculate the spectra of synchrotron, Compton and Bremsstrahlung emission in the following sections.

In a particular case when the shape of the particle spectrum is affected by the effects of cooling

$$\Gamma_e = \Gamma_{inj} + \gamma_{cool} - 1 \tag{2.39}$$

the emission spectrum is independent on the energy scaling of the cooling rate $\gamma_{cool}$:

$$\phi(E_\gamma) \sim E_\gamma^{\frac{2 - 2\sigma - \Gamma_{inj}}{\sigma}} \tag{2.40}$$

Examples of powerlaw (or cut-off powerlaw) spectra of emission from a distribution of high-energy particles could be found in Figs. 2.3, 2.12. Publicaitons in X-ray and $\gamma$-ray astronomy often give representation of the spectrum in the form

$$\begin{aligned}
&\frac{dN_\gamma}{dE}(E_\gamma) \sim \phi(E_\gamma), \text{ "differential spectrum" or} \\
&E_\gamma\frac{dN_\gamma}{dE}(E_\gamma) \sim E_\gamma\phi(E_\gamma), \text{ "photon spectrum" or} \\
&E_\gamma^2\frac{dN_\gamma}{dE}(E_\gamma) \sim E_\gamma^2\phi(E_\gamma), \text{ "spectral energy distribution"}
\end{aligned} \tag{2.41}$$

The first representation for the photon flux, in units of "photons/(cm$^2$s eV)" is called the "differential spectrum", i.e. it is the photon count rate per unit detector area per unit time and *per unit energy interval*. The second representation provides a fair judgement of the signal statistics in different energy bands, because it gives the count rate of photons per unit detector area *per decade of energy*. Finally, the third representation, often called "Spectral Energy Distribution" or SED of the source, provides an estimate of the " emitted power per energy decade". This representation is useful for building physical models of the sources. It allows to judge in which energy band most of the source power is emitted.

| Cooling law: | | $\dot{E} \propto E_e^{\gamma_{cool}}$ |
|---|---|---|
| Relation between photon and electron energies: | | $E_\gamma \propto E_e^{\sigma}$ |
| Electron spectrum: | | $dN_e/dE_e \propto E_e^{-\Gamma}$ |
| Emission spectrum: | | $dN_\gamma/dE_\gamma \propto E_\gamma^{\frac{\gamma_{cool}+1-\Gamma_e-2\sigma}{\sigma}}$ |
| Evolution of electron spectrum: | | $\Gamma_{inj} \to \Gamma_{inj} + \gamma_{cool} - 1$ |
| | $\gamma_{cool}$ | $\sigma$ |
| curvature radiation | 4 | 3 |
| synchrotron radiation | 2 | 2 |
| inverse Compton (T) | 2 | 2 |
| inverse Compton (KN) | 0 | 1 |
| Bremsstrahlung | 1 | 1 |

## 2.5 Cyclotron emission / absorption

Considering the curvature radiation, we have assumed that the emitting charged particle moves along a circular trajectory of an arbitrary radius $R$. In the particular example of pulsars, this radius was estimated to be comparable to the size of the emitting system (about 10 km, which is the size of the neutron star). Another possibility is that the emitting particles are confined to much smaller distance scales than the entire source size.

This is the case for the particles moving in magnetic fields. In this case particles spiral along magnetic field lines, being confined within the distance equal to the gyroradius $R_L$. The gyroradius is readily found from the second law of Newton,

$$ma = \frac{mv^2}{R_L} = evB \tag{2.42}$$

which gives

$$R_L = \frac{mv}{eB} \tag{2.43}$$

The angular frequency of gyration is just

$$\omega_B = \frac{v}{R_L} = \frac{eB}{m} \simeq 12 \left[\frac{B}{10^{12}\ \mathrm{G}}\right] \left[\frac{m}{m_e}\right]^{-1}\ \mathrm{keV} \tag{2.44}$$

Non-relativistic particles moving in magnetic field emit dipole radiation at the frequency (energy) $\omega_B$. This emission is called cyclotron emission. This emission is difficult to observe (remember that astronomical observations start from radio band, in the frequency range starting from 100 MHz, which correspond to photons of the energies higher than $10^{-6}$ eV. If the magnetic field in an object is lower than $\sim 100$ G, the cyclotron emission is not observable. At the same time, strong magnetic fields in astronomical sources might reveal themselves through the characteristic cyclotron emission features.

### 2.5.1 Astrophysical example (accreting pulsars)

Such features are observed in the spectra of X-ray accreting pulsars. These systems contain magnetised neutron stars, but there is no particle acceleration in the pulsar magnetosphere. Instead, there is ionised matter right next to the surface of the neutron star. The neutron star is magnetised, so that electrons and protons/nuclei gyrate in the magnetic field. The magnetic field is the dipole field of the star, so it is very homogeneous (on small distance scales).

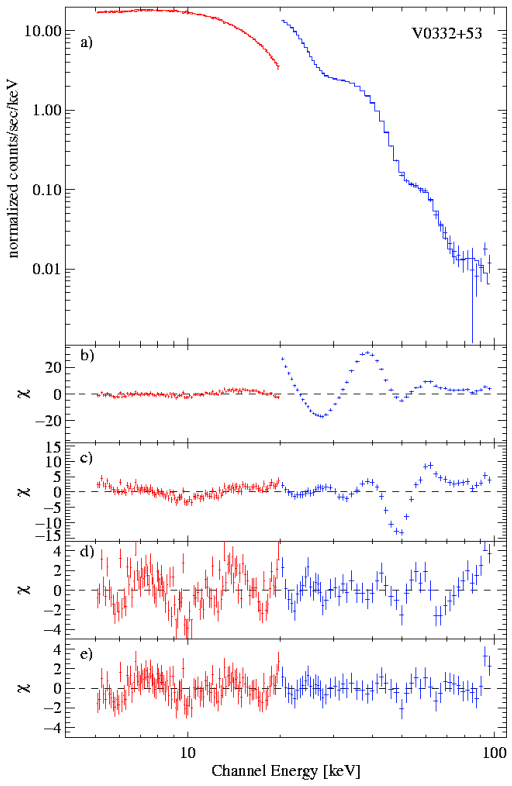


Figure 2.5: Spectrum of X-ray accreting pulsar V 0332+53, showing a series of cyclotron lines [10]. Upper panel shows the overall spectrum, lower panels show the deviations of the data from the model, first without inclusion of the lines, and then after addition of one, two three cyclotron lines. The spectrum is in "normalised counts" units, which is just a histogram of photon counts in a given energy bin. It is different from the conventional spectra in physical units of flux (e.g. "photons per cm$^2$ and second"). Conversion from "normalised counts" to physical units requires a knowledge of energy response of the detector.

The gyroradius of electrons in the strong dipole field of the neutron star is extremely small:

$$R_L = \frac{m_e v}{eB} \simeq 10^{-9} v \left[\frac{B}{10^{12}\ \mathrm{G}}\right]^{-1}\ \mathrm{cm} \qquad (2.45)$$

This is a microscopic radius which is comparable to the deBroglie wavelength

$$\lambda_{dB} = \frac{1}{m_e v} \simeq 4 \times 10^{-11} v^{-1} \mathrm{cm} \qquad (2.46)$$

If

$$B > \frac{m_e^2 v^2}{e} \simeq 4 \times 10^{13} v^2\ \mathrm{G} \qquad (2.47)$$

the spread of electron wavefunction is larger than the gyroradius. This means that the motion of electrons in magnetic field should be considered as a quantum mechanical problem (see Exercise 2.4). In this case the energy levels of particle are discrete (if there is no momentum component $p_z$ in the direction of magnetic field. These levels are called Landau levels:

$$E_n - \frac{p_z^2}{2m} = (n + 1/2)\frac{eB}{m} = (n + 1/2)\omega_B \qquad (2.48)$$

where $n$ is an integer number.

Similarly to electrons in atoms, the spectra of emission and absorption from electrons at Landau levels are discrete. Being the spectra of harmonic oscillators, they are formed by series of equidistant lines. Measurement of the line energies provides a measurement of the magnetic field close to the neutron star surface. Fig. 2.5 shows an example of observation of cyclotron line series in the spectrum of one of the accreting pulsars, V 0332+53, done by INTEGRAL telescope [10].

The line energies are in the 10 keV band. From Eq. (2.44) we infer that the magnetic field strength in the photon emission region is about $10^{12}$ G. This magnetic field is much stronger than the fields which are encountered in laboratory conditions (which are $\lesssim 10^5$ G for the strongest man-made magnets). They are also much higher than the fields of normal stars. The magnetic fields at the surface of the Sun reach at most kG strengths.

## 2.6 Synchrotron emission

Cyclotron emission / absorption is produced by non-relativistic particles gyrating in magnetic field. If the particles are relativistic, the properties of the dipole electromagnetic radiation due to the gyration in magnetic field change.

Basic relations for the energy of synchrotron photons and power of synchrotron emission could be found directly from the formulae for dipole and, in particular, for curvature radiation simply via

substitution of the relativistic expression for the gyroradius (the relativistic analog of Eq. (2.43))

$$R_L = \frac{E_e}{eB} \simeq 3 \times 10^7 \left[\frac{E_e}{10^{10}\ \mathrm{eV}}\right] \left[\frac{B}{1\ \mathrm{G}}\right]^{-1}\ \mathrm{cm} \tag{2.49}$$

instead of an arbitrary $R$ in the corresponding formulae. This exercise with Eq. (2.24) gives

$$\epsilon_{synch} = \frac{\gamma^3}{R_L} = \frac{eBE_e^2}{m_e^3} \simeq 5 \left[\frac{B}{1\ \mathrm{G}}\right] \left[\frac{E_e}{10^{10}\ \mathrm{eV}}\right]^2 \mathrm{eV} \tag{2.50}$$

for the energy of synchrotron photons. Note that contrary to the energy of curvature radiation photons, which scales as $E_e^3$, the energy of the synchrotron photons grows only as $E_e^2$ with the increase of the electron energy. This is because the curvature radius of electron trajectory expands with increasing electron energy.

Substituting $R_L$ at the place of $R$ in Eq. (2.25) we find the energy loss rate on the synchrotron emission:

$$-\frac{dE_e}{dt} \simeq \frac{2}{3}\frac{e^4B^2E_e^2}{m_e^4} \simeq 4 \times 10^5 \left[\frac{B}{1\ \mathrm{G}}\right]^2 \left[\frac{E_e}{10^{10}\ \mathrm{eV}}\right]^2\ \mathrm{eV/s} \tag{2.51}$$

The energy loss rate grows only as $E_e^2$ with the increase of the electron energy. The synchrotron loss time is then

$$t_{synch} = \frac{E_e}{-dE_e/dt} = \frac{3m_e^4}{2e^4B^2E_e} \simeq 2 \times 10^4 \left[\frac{B}{1\ \mathrm{G}}\right]^{-2} \left[\frac{E_e}{10^{10}\ \mathrm{eV}}\right]^{-1}\ \mathrm{s} \tag{2.52}$$

We could also re-use the results of Section 2.4 to find the spectrum of a broad band distribution of electrons, e.g. from a powerlaw type spectrum with the slope $\Gamma_e$:

$$\frac{dN_e}{dE_e} \sim E_e^{-\Gamma_e} \tag{2.53}$$

Repeating the calculation leading to Eq. 2.38 we find that for the synchrotron emission both parameters $\gamma_{cool}$ and $\sigma$ are equal to 2, so that the spectrum of synchrotron emission has the photon index

$$\phi(E_\gamma) = \frac{dN_\gamma}{dE_\gamma} \sim E_\gamma^{-\Gamma_{synch}}, \quad \Gamma_{synch} = \frac{\Gamma_e + 1}{2} \tag{2.54}$$

We could also re-use the formulae for the evolution and steady state spectra of particles with account of energy loss, derived in Section 2.3, to understand the influence of the synchrotron energy loss on the spectrum of high-energy electrons. The evolution of the spectrum of electrons is governed by Eq. (2.31) with the energy loss rate being due to the synchrotron emission, Eq. (2.51). In the absence of escape, its general steady state solution has the form (2.32).

In the particular case of mono energetic injection, $Q(E) \sim \delta(E - E_0)$, the solution has the form (2.33), which in the case of $\dot{E} \sim E^2$ is

$$\frac{dN_e}{dE_e} \sim \begin{cases} E_e^{-2}, & E < E_0 \\ 0, & E > E_0 \end{cases} \tag{2.55}$$

More generally, if the acceleration process results in injection of electrons in the energy range above some limiting lowest energy (the injection spectrum has a low-energy cut-off), synchrotron cooling leads to formation of an $E^{-2}$ type spectrum of the "cooling tail" below the minimal injection energy.

The synchrotron emission from the "cooling tail" has a powerlaw-type spectrum with the slope $\Gamma_{synch} = (2+1)/2 = 1.5$, see Eq. (2.54).

Another useful example if that of the effect of synchrotron energy loss on the powerlaw type injection spectrum $Q(E) \sim E^{-\Gamma_{inj}}$. In this case, substituting $q_{cool} = 2$ into Eq. (**??**) we find

$$\frac{dN_e}{dE_e} \sim E_e^{-(\Gamma_{inj}+1)} \tag{2.56}$$

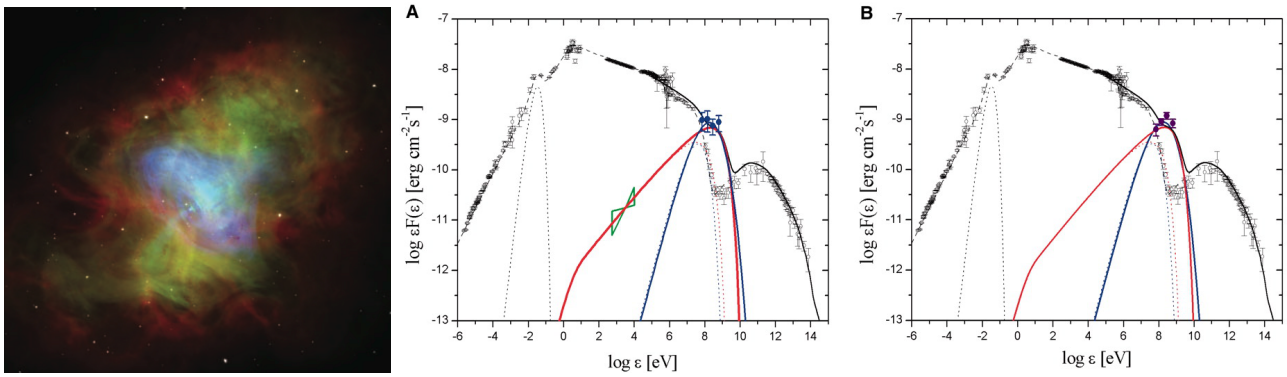


Figure 2.6: Multiwavelength image (left) and spectrum (right) of the Crab pulsar wind nebula. In the image (from [11]): blue colour is X-ray, green is in visible light and red is radio emission. In the spectrum (from [12]) black data points show time-averaged spectrum of the source. Blue and violet points show examples of spectra during GeV band flares.

Thus, synchrotron cooling leads to a "softening" of the initial injection spectrum $\Gamma_{inj} \to \Gamma_{inj}+1$. This corresponds to a larger and larger "pile up" of the cooled electrons at lower and lower energies. Such a "pile up" could be understood qualitatively if one recalls that the kinetic equation (2.31) describes motion of particles in energy space. The speed of this motion, $\dot{E}$ is decreasing with the decrease of the energy, so that the particles get gradually "stuck" while movingg to lower energy bins. This leads to accumulation of larger number of particles in lower energy bins.

Suppose that the injection spectrum is an $E^{-2}$ type powerlaw (this is typical slope of the spectrum resulting from the shock acceleration, as we will see later on). Synchrotron cooling would soften the spectrum down to an $E^{-3}$ type spectrum. The photon index of the synchrotron emission from the cooled distribution of electrons would then have the slope $\Gamma = (3+1)/2 = 2$.

### 2.6.1 Astrophysical example (Crab Nebula)

A prototypical example of the high-energy source is Crab nebula, which is a nebular emission around a young ($10^3$ yr old) pulsar. It is one of the brightest $\gamma$-ray sources on the sky and serves as a calibration target for most of the $\gamma$-ray telescopes. The spectrum of emission from the Crab nebula spans twenty decades in energy, from radio (photon energies $10^{-6}$ eV) up to the Very-High-Energy $\gamma$-ray (photon energies up to 100 TeV) band. Large, parsec-scale size and moderate distance (2 kpc) to the nebula enable detailed imaging of the source in a range of energy bands, from radio to X-ray. The composite radio-to-X-ray image of the nebula is shown in Fig. 2.6, top panel.

Radio to X-ray and up to GeV $\gamma$-ray emission from the nebula presents a composition of several broad powerlaw-type continuum spectra, with the photon indices changing from $\Gamma \simeq 1.3$ in the radio-to-far-infrared band to $\Gamma \simeq 2.2$ in the 1-100 MeV band. Such powerlaw type spectra extending down to the infrared and radio domains are commonly interpreted as being produced by the synchrotron emission mechanism.

Measurement of the slope of the synchrotron spectrum provides information on the shape of the parent electron spectrum, which is of a "broken powerlaw" type. Electrons responsible for the emission in the radio-to-visible energy range are characterised by a spectrum with the slope close to $\Gamma_e \simeq 2$, since the synchrotron spectrum has the slope close to $\Gamma_{synch} = 1.5$ (see Eq. (2.54)). One could tentatively interpret this $E^{-2}$ type spectrum either as an un-cooled injection spectrum of electrons, or as a low energy "cooling tail" formed below the low-energy cut-off in the injection spectrum of electrons, see Eq. (2.55).

Softening of the spectrum above $\sim 10$ eV might be interpreted as the effect of synchrotron cooling on the initial electron injection spectrum. The "cooling break" in the spectrum of electrons, by

$\Delta\Gamma_e = 1$ occurs at the energy at which the cooling time is approximately equal to the time since the start of injection of high-energy electrons. Electrons with energies lower than the break energy did no have time to loose their energy since the beginning of injection and their spectrum is the unchanged injection spectrum.

Let us assume that the break observed in the spectrum of synchrotron emission in the Crab nebula is due to the "cooling break' in the spectrum of electrons. The time passed since the start of injection in the nebula is the age of the system, which is about $10^3$ yr (i.e. the time since the supernova explosion which led to formation of the system). The synchrotron cooling time is given by Eq. (2.52):

$$t_{synch} \simeq 10^3 \left[\frac{B}{100\ \mu\mathrm{G}}\right]^{-2} \left[\frac{E_e}{10^{12}\ \mathrm{eV}}\right]^{-1}\ \mathrm{yr} \tag{2.57}$$

Thus, an estimate of the cooling time provides a constraint on the energy of electrons responsible for the synchrotron emission in the 1-10 eV range and the strength of magnetic field in the nebula. The energy of synchrotron photons is also determined by the energy of electrons and the strength of the magnetic field, but in a different combination, see Eq. (2.50):

$$\epsilon_{synch} \simeq 5 \left[\frac{B}{100\ \mu\mathrm{G}}\right] \left[\frac{E_e}{10^{12}\ \mathrm{eV}}\right]^{2} \mathrm{eV} \tag{2.58}$$

combining the two measurements (of $\epsilon_{synch}$ and $t_{synch}$) we find that if the break in the spectrum of synchrotron emission from the Crab nebula is due to the synchrotron cooling effect on electron spectrum, the magnetic field in the nebula should be close to

$$B \sim 100\ \mu\mathrm{G} \tag{2.59}$$

The energies of electrons for which the cooling time is about the age of the Crab nebula are

$$E_{e,break} \sim 10^{12}\ \mathrm{eV} \tag{2.60}$$

From Fig. (2.6) one could see that the spectrum of synchrotron emission has a high-energy cut-off in the 100 MeV range, where is sharply declines. Electrons which produce synchrotron emission in the 100 MeV energy range should have energies (see Eq. (2.58))

$$E_{e,max} \sim 1 - 10\ \mathrm{PeV} \tag{2.61}$$

range. This shows that Crab nebula hosts a remarkably powerful particle accelerator. For comparison, the energies of particles accelerated in the most powerful man-made accelerator machine, the Large Hadron Collider, are in the 10 TeV range, which is three orders of magnitude lower.

Up to recently, Crab Nebula was believed to be a non-variable source and was conventionally used as a calibration sources for X-ray and $\gamma$-ray telescopes, due to its high flux and stability. However, recent observations by *Fermi* and *AGILE* $\gamma$-ray telescopes have revealed variability of the $\gamma$-ray emission from Crab, in the form of short powerful flares, during which the GeV flux of the source rises by an order of magnitude, see Fig. 2.6. These flares occur at the highest energy end of the synchrotron spectrum and have durations in the $t_{flare} \sim 1 - 10$ d$\sim 10^5 - 10^6$ s range. Comparing the synchrotron cooling times of the 1-10 PeV electrons with the duration of the flares, one finds

$$t_{synch} \simeq 24 \left[\frac{B}{100\ \mu\mathrm{G}}\right]^{-2} \left[\frac{E_e}{10^{16}\ \mathrm{eV}}\right]^{-1}\ \mathrm{d} \geq t_{flare} \tag{2.62}$$

This implies that the flares occur in the innermost part of the nebula, in the regions with higher magnetic field ($B \sim 500\ \mu$G), otherwise, long synchrotron cooling time would smooth the flare lightcurve on the time scale $t_{synch}$ and the flare would not have 1 d duration.

The flaring time scale is most probably directly related to the time scale of an (uncertain) acceleration process, which leads to injection of multi-PeV electrons in the nebula. We will come back to this issue later on in the discussion of the properties of pulsars and their nebulae.

## 2.7 Compton scattering

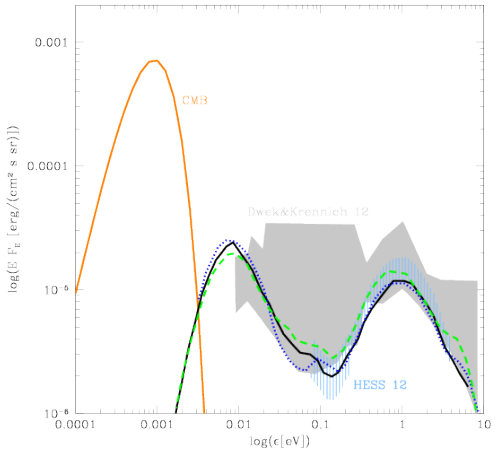


Figure 2.7: The spectrum of Extragalactic Background Light. Grey band shows the range of uncertainties of currently existing measurements.

The spectrum of emission from the Crab nebula has apparently two "bumps": one starting in the radio band and ending in the GeV band and the other spanning the 10 GeV-100 TeV needy range with a peak in at $\sim$ 100 GeV. We have interpreted the radio-to-$\gamma$-ray bump as being the result of synchrotron emission from high-energy electrons in the source. The synchrotron emission is an "inevitable" radiative loss channel in a wide range of astronomical sources, because most of the known sources possess magnetic fields. There is practically no place in the Universe without magnetic field.

Similarly to magnetic fields, the whole Universe is also filled with radiation fields. Radiation was generated by the hot Early Universe. This relic radiation survives till today in the form of Cosmic Microwave Bakcground (CMB). CMB is thermal radiation with temperature $T_{CMB} \simeq 2.7$ K and its present in equal amounts everywhere in the Universe. The spectrum of CMB is the Planck spectrum. Its energy density is

$$U_{CMB} = \frac{\pi^2}{15} T^4 \simeq 0.25 \left[\frac{T_{CMB}}{2.7 \text{ K}}\right]^4 \frac{\text{eV}}{\text{cm}^3} \tag{2.63}$$

and the number density of CMB photons is

$$n_{CMB} = \frac{2\zeta(3)}{\pi^2} T^3 \simeq 4 \times 10^2 \left[\frac{T_{CMB}}{2.7 \text{ K}}\right]^3 \frac{\text{ph}}{\text{cm}^3} \tag{2.64}$$

Apart from the universal CMB photon background, radiation fields are generated by collective emission from stars and dust in all galaxies over the entire galaxy evolution span. This leads to production of the so-called "Extragalactic Background Light" with a characteristic two-bump spectrum shown in Fig. 2.7. The bump at the photon energy $\sim$ 1 eV is produced by the emission form stars, the bump at $10^{-2}$ eV is due to the scattering of starlight by the dust. Fig. 2.7 shows the level of the starlight and dust emission averaged over the entire Universe. Inside the galaxies, the densities of both the starlight and dust photon fields are enhanced by several orders of magnitude.

Still denser photon fields exist inside astronomical sources, e.g. close to the stars or in the nuclei of active galaxies.

High-energy particles propagating through the photon backgrounds could occasionally collide with the low energy photons and loose / gain energy in the scattering process. This phenomenon is called Compton scattering.

The high-energy bump in the spectrum of Crab nebula is produced by a variety of the Compton scattering process in which high-energy electrons collide with low energy photons present in the nebula. This results in the transfer of energy from electrons to photons so that the low-energy photons are converted into high-energy $\gamma$-rays and electrons loose their energy. This process is called "inverse Compton scattering". In this section we consider different aspects of the Compton scattering process.

### 2.7.1 Thomson cross-section

The process of charged particle – photon scattering could be described within classical mechanics as re-radiation of waves by the particle accelerated by the electric field of the incident electromagnetic wave.

As an initial example, we consider this process for a non-relativistic electron. The force acting on the charged particle is the Lorentz force

$$\vec{F} = e(\vec{E} + [\vec{v} \times \vec{B}]) \tag{2.65}$$

The wave has electric and magnetic fields of comparable strength. This means that the term proportional to the magnetic field in the Lorentz force is much smaller than the electric field term, because we consider $v \ll 1$. Let us consider the wave propagating in $z$ direction, so that the electric and magnetic field vectors are in the $xy$ plane. The components of acceleration of the particle are

$$\begin{aligned} a_x &\simeq \frac{e}{m} E_x \\ a_y &\simeq \frac{e}{m} E_y \end{aligned} \tag{2.66}$$

For a linearly polarised plane wave, the electric field components at a given position vary as

$$E_x = E_0 \sin(\omega t + \phi) \tag{2.67}$$

where $\omega$ is the wave angular frequency. Thus, $a_x$ oscillates periodically.

Using the Larmor formula, we find the power of emission by the accelerated particle

$$\left\langle \frac{d\mathcal{E}}{dt} \right\rangle = \frac{2}{3} e^2 \left\langle a_x^2 \right\rangle = \frac{2}{3} \frac{e^4}{m^2} \left\langle E_x^2 \right\rangle \tag{2.68}$$

(we introduce curly font for the emitted energy, to avoid confusion with electric field). Time averaged emission power depends on

$$\left\langle E_x^2 \right\rangle = \frac{\omega}{2\pi} \int_0^{2\pi/\omega} E_0^2 \sin^2(\omega t + \phi) dt = \frac{2E_0^2}{\pi} \int_0^{\pi/2} \sin^2 x dx = \frac{E_0^2}{2} \tag{2.69}$$

Substituting into Eq. (2.68) we find

$$\left\langle \frac{d\mathcal{E}}{dt} \right\rangle = \frac{1}{3} \frac{e^4}{m^2} E_0^2 \tag{2.70}$$

In scattering theory, the cross-section is defined as the ratio of the emitted energy to the incident energy flux $\vec{S}$

$$\sigma = \frac{d\mathcal{E}/dt}{|\vec{S}|} \tag{2.71}$$

The energy flux of the incident wave is given by the Poynting vector

$$\left\langle \vec{S} \right\rangle = \frac{\left\langle \vec{E} \times \vec{B} \right\rangle}{4\pi} = \frac{E_0^2}{8\pi} \tag{2.72}$$

substituting this into expression for the cross-section we find

$$\sigma = \frac{d\mathcal{E}/dt}{|\vec{S}|} = \frac{8\pi}{3} \frac{e^4}{m^2} \tag{2.73}$$

If the scattering centre is an electron, $e$ is the electron charge and $m = m_e$ is its mass. In this case the cross-section is a fundamental constant called Thomson cross-section:

$$\sigma_T = \frac{8\pi e^4}{3m_e^2} \simeq 6.65 \times 10^{-25} \text{ cm}^2 \tag{2.74}$$

Using the definition of $\sigma_T$ one could rewrite the expression for the power of emission as

$$\frac{d\mathcal{E}}{dt} = \frac{8\pi e^4}{3m_e^2} \frac{E_0^2}{8\pi} = \sigma_T U_{rad} \tag{2.75}$$

where we have introduced the notation for the energy density of the incident radiation

$$U_{rad} = \left\langle \frac{\vec{E}^2}{8\pi} + \frac{\vec{B}^2}{8\pi} \right\rangle = \frac{E_0^2}{8\pi} \tag{2.76}$$

### 2.7.2 Example: Compton scattering in stars. Optical depth of the medium. Eddington luminosity

The most widespread example of Compton scattering in astronomy is the scattering of photons inside stars. The nuclear reactions which power stellar activity proceed most efficiently deep in the stellar cores, where temperatures are significantly higher than at the stellar surface. However, we are not able to observe directly radiation from the nuclear reactions, because the star is "opaque" to the radiation. The process which prevents photons produced deep inside the stars from escaping is the Compton scattering.

Let us take the Sun as an example. The average density of the Sun with the size $R = R_\odot$ is

$$n = \frac{M_\odot}{(4\pi/3)R^3 m_p} \simeq 10^{24} \left[\frac{R}{R_\odot}\right]^{-3} \text{ cm}^{-3} \tag{2.77}$$

From the definition of the scattering cross-section, we find that the mean free path of photons with respect to collisions with electrons inside the Sun is just

$$\lambda = \frac{1}{\sigma_T n} \simeq 1 \text{ cm} \tag{2.78}$$

This mean free path is much shorter than the distance of the order of the size of the Sun $R_\odot \simeq 7 \times 10^{10}$ cm which the photon needs to cross before leaving the surface of the Sun. Since $\lambda \ll R_\odot$, none of the photons produced in the core is able to escape. The source is opaque to photons. The opacity of the source of the size $R$ is often measured in terms of the optical depth, which is, by definition

$$\tau = \frac{R}{\lambda} \tag{2.79}$$

In the case of the Sun we find that $\tau \sim 10^{11}$. The optical depth also describes the law of attenuation of a directed beam of photons (or of any other particles) by the scattering in the medium. The number of particles in the beam in $z$ direction entering the medium at $z = 0$ decreases with distance as

$$N(z) = N_0 \exp\left(-\tau(z)\right), \tau(z) = \frac{z}{\lambda} \tag{2.80}$$

If we assume that Compton scattering results in random changes of the direction of motion of photons, we could describe the process of escape of photons from inside the star as a random walk or diffusion in 3d space. The law of diffusion allows to estimate the time needed for photons to escape from the core

$$t = \frac{R^2}{\lambda} = \tau \frac{R}{c} \simeq 10^{11} \left[\frac{R}{R_\odot}\right]^{-1} \text{ s} \tag{2.81}$$

Thus, Compton scattering slows down the radiative transfer from the core to the surface of the stars.

Compton scattering is important in stars in still another aspect. Compton scattering of photons on electrons results in energy transfer between the two particles. In this way a flux of radiation from a given direction produces pressure on the plasma (radiation pressure). If we imagine a low energy photon bouncing from an electron, the change of momentum of the photon in result of scattering is about the momentum itself, $\Delta p \sim p \sim \epsilon$, where $\epsilon$ is the photon energy. A flux of photons with density $n$ transfers an energy to each electron in the plasma at a rate comparable to the power of the scattered radiation

$$\frac{d\mathcal{E}}{dt} \simeq \epsilon n \sigma_T \tag{2.82}$$

This energy transfer is the result of action of the radiation force $d\mathcal{E} = F_{rad} dt$.

Sun-like stars are supported by the balance of gravity force and pressure of the stellar plasma. However, in massive stars with much higher luminosity than that of the Sun, the force due to the

radiation pressure competes with the gravity and the equilibrium configuration of the star is supported by the balance of gravity and radiation pressure force

$$\frac{G_N M m_p}{R^2} \simeq \epsilon n \sigma_T \tag{2.83}$$

(we assume that the number of protons and electrons in the star is the same). The strongest radiation pressure force is acting on electrons, stronger gravity force is acting on protons. Expressing the density of radiation through the luminosity $L$

$$\epsilon n = \frac{L}{4\pi R^2} \tag{2.84}$$

and substituting into above equation we find an expression for $L$ through the mass of the star

$$L_{Edd} = \frac{4\pi G_N M m_p}{\sigma_T} \simeq 10^{38} \left[\frac{M}{M_\odot}\right] \text{ erg/s} \tag{2.85}$$

This mass-dependent luminosity, called Eddington luminosity, is, in fact an upper limit on the luminosity of a self-gravitating object. No persistent astronomical source of the mass $M$ could have luminosity higher than $L_{Edd}$, because otherwise the source would be disrupted by the radiation pressure force. This limit applies not only to the stars, but also for numerous other source types and we will see several examples of the use of the Eddington limit later on in the course.

### 2.7.3 Angular distribution of scattered waves

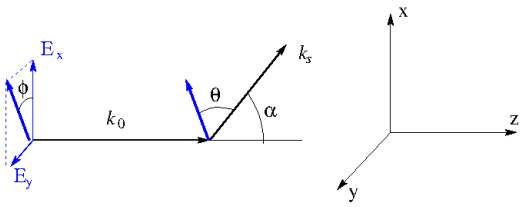


Figure 2.8: Geometry of Compton scattering.

The angular distribution of the waves emitted by a non-relativistic scattering centre could be found from a general formula for the dipole radiation from non-relativistic particle (2.9)

$$\frac{d\mathcal{E}}{dtd\Omega} = \frac{e^2}{4\pi}|a|^2 \sin^2\theta \tag{2.86}$$

where $\theta$ is the angle between the direction of acceleration and the direction of the scattered wave. To calculate this angle, we choose the coordinate system in the following way (see Fig. 2.8). The $z$ axis points in the direction of the incident wave. The $xz$ plane contains the wave vector of the incident wave, $\vec{k}_0$ and the wave vector of the scattered wave, $\vec{k}_s$. The $y$ axis is orthogonal to the $xz$ plane. In such notations we rewrite the above equation as

$$\frac{d\mathcal{E}}{dtd\Omega} = \frac{e^2}{4\pi}\left|\vec{a}\times\vec{k}_s\right|^2 = \frac{e^4}{4\pi m^2}\left|\vec{E}\times\vec{k}_s\right|^2 = \frac{e^4}{4\pi m^2}\left|(\vec{E}_x+\vec{E}_y)\times\vec{k}_s\right|^2 \tag{2.87}$$

where $\vec{E}_x, \vec{E}_y$ are components of the electric field along x and y axes. The vector $\vec{E}_x \times \vec{k}_s$ is directed along the $y$ axis, while the vector $\vec{E}_y \times \vec{k}_s$ lies in the $xz$ plane. They are orthogonal to each other. This implies that the square of the norm of their sum is the sum of their norms square

$$\frac{d\mathcal{E}}{dtd\Omega} = \frac{e^4}{4\pi m^2}\left(\left|\vec{E}_x\times\vec{k}_s\right|^2 + \left|\vec{E}_y\times\vec{k}_s\right|^2\right) \tag{2.88}$$

$\vec{E}_y$ is orthogonal to $\vec{k}_s$, so that their vector product is just the product of the norms

$$\left\langle\left|\vec{E}_y\times\vec{k}_s\right|^2\right\rangle = \frac{1}{2}E_{0,y}^2 \tag{2.89}$$

where we have used the fact that the time averaging of the electric field norm square results in the factor 1/2 (see Eq. (2.69)). Introducing the angle $\alpha$ between the direction of the incident and scattered wave, one could find that $\theta = \pi/2 - \alpha$. Thus

$$\left\langle \left| \vec{E}_x \times \vec{k}_s \right|^2 \right\rangle = \frac{1}{2} E_{0,x}^2 \cos^2 \alpha \tag{2.90}$$

Let us assume that the incident wave is unpolarised, so that $E_{0,x} \simeq E_{0,y} \simeq E_0/\sqrt{(2)}$ for any choice of the scattering direction $\vec{k}_s$. Then we could add the two terms together to find

$$\frac{d\mathcal{E}}{dtd\Omega} = \frac{e^4 E_0^2}{16\pi m^2} \left(1 + \cos^2 \alpha\right) \tag{2.91}$$

Division by the energy flux of the incident wave gives the differential cross-section of Compton scattering

$$\frac{d\sigma}{d\Omega} = \frac{d\mathcal{E}/(dtd\Omega)}{S} = \frac{e^4}{2m^2}(1 + \cos^2 \alpha) \tag{2.92}$$

As a verification, we could find that integrating the differential cross-section over the solid angle gives the Thomson cross-section

$$\int d\Omega \frac{d\sigma}{d\Omega} = \sigma_T \tag{2.93}$$

For a polarised wave, the amplitude of Compton scattering depends not only on the angle $\alpha$, but also on the azimuthal angle $\phi$, since $\theta$ is a function of both $\alpha$ and $\phi$. This fact could be used to measure the polarisation of the incident radiation. It is indeed used in telescopes for this purpose. An example of a "gamma-ray polarimeter" based on this principle is given by POLAR detector for the measurement of polarisation of Gamma-ray bursts. We will stop at this issue in a subsection discussing Compton telescopes later on.

### 2.7.4 Thomson scattering

To find the energy transfer from electron to photon or vise versa we write down the energy-momentum conservation law

$$\underline{p}_{e,i} + \underline{p}_{\gamma,i} = \underline{p}_{e,f} + \underline{p}_{\gamma,f} \tag{2.94}$$

where the subscripts $e, \gamma$ refer to electron and photon and $i, f$ are for initial and final state. We could re-express this as

$$m_e^2 = |p_{e,f}|^2 = (\underline{p}_{e,i} + \underline{p}_{\gamma,i} - \underline{p}_{\gamma,f})^2 = m_e^2 + 2(\underline{p}_{e,i}\underline{p}_{\gamma,i} - \underline{p}_{e,i}\underline{p}_{\gamma,f} - \underline{p}_{\gamma,i}\underline{p}_{\gamma,f}) \tag{2.95}$$

Let us consider the system of reference where the electron is initially at rest, that is $\underline{p}_{e,i} = (m_e, 0, 0, 0)$ in components. We could choose the $x$ axis along the initial direction of motion of photon in this system so that $\underline{p}_{\gamma,i} = \epsilon_i(1, 1, 0, 0)$. Then we choose the $y$ axis orthogonal to $x$ in the plane of scattering, so that $\underline{p}_{\gamma,f} = \epsilon_f(1, \cos\alpha, \sin\alpha, 0)$, where we have introduced the initial and final energies of the photon, $\epsilon_i, \epsilon_f$. Substituting the component in the last equation we find

$$m_e\epsilon_i = m_e\epsilon_f + \epsilon_i\epsilon_f(1 - \cos\alpha) \tag{2.96}$$

or, reexpressing $\epsilon_f$,

$$\epsilon_f = \frac{\epsilon_i}{1 + \frac{\epsilon_i}{m_e}(1 - \cos\alpha)} \tag{2.97}$$

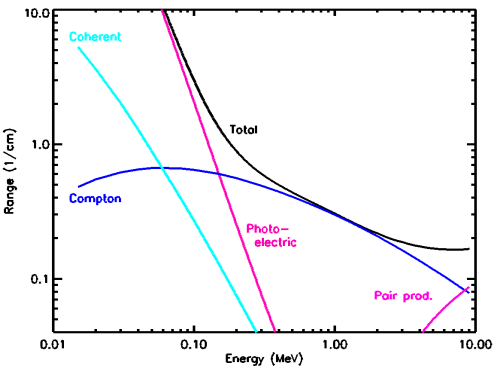


Figure 2.9: Cross-section of interaction of photons with medium (Germanium) as a function of energy.

For example, for the scattering at zero angle $\alpha = 0$ we find
that there is no energy transfer between electron and photon: $\epsilon_i = \epsilon_f$. For the scattering at $\alpha = \pi$ we have $\epsilon_f = \epsilon_i/(1 + 2\epsilon_i/m_e) < \epsilon_i$. In this case the energy of photon is used on the recoil of electron.

Scattering of low energy photons by non-relativistic electrons is characterised by tiny changes of the photon energy, so that $\epsilon_f \simeq \epsilon_i$, photons bounce nearly elastically from electrons. This limits is called Thomson scattering (e.g. close to the surface of the star).

### 2.7.5 Example: Compton telescope(s)

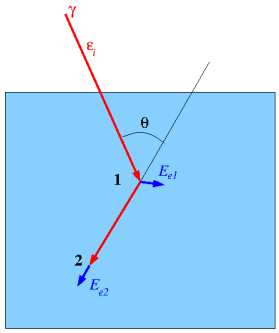


Figure 2.10: Principle of operation of Compton telescope

The above Eq. (2.97) is the main ingredient in the principle of operation of the so-called Compton telescopes, i.e. telescopes which detect $\gamma$-rays though the Compton scattering effect. Imagine a setup in which a moderate energy $\gamma$-ray enters a detection volume and scatters on an electron at a point 1 as shown in Fig. 2.10.

The $\gamma$-ray transfers a part of its energy $E_{e1} = \epsilon_f - \epsilon_i$ to an electron. Depending on the choice of the detection medium, the energy of electron can be measured in a variety of ways. For example, if the medium is a scintillator, the scintillation signal could be sampled by photomultiplier sensors. Otherwise, if the medium is a semiconductor, electron excitation will lead to production of electron-hole pairs which could then be sampled in the form of a current flowing through an electric circuit including the detector.

The scattered photon continues its path an could interact second time inside the detector medium at the point 2. The energy of the scattered photon $\epsilon_f$ is lower than $\epsilon_i$ and the second interaction could, with a good chance, be photoelectric absorption, rather than Compton scattering. This is because the Compton scattering dominates the photon-medium interaction cross-section only in a narrow energy interval from $\epsilon_i \sim 100$ keV to about the rest energy of electron, $\epsilon_i \sim m_e = 511$ keV. At lower energies $\epsilon_i \lesssim 100$ keV the highest interaction cross-section is that of the photoelectric effect, see Fig. 2.9 for an example of the Germanium (semiconductor) detection medium.

Photoelectric absorption also transfers the photon energy to (another) which gets the energy $E_{e2} = \epsilon_f$. Measuring $E_{e2}$ in the same way as $E_{e1}$ one could constrain parameters of Compton scattering at point 1. Indeed, the unknown parameters are the photon energy $\epsilon_i$ and the scattering angle $\alpha$. Measuring $E_{e2} = \epsilon_f$ and $E_{e1} = \epsilon_i - \epsilon_f$ one could find both $\epsilon_i$ and $\alpha$ from Eq. (2.97).

Knowing the scattering angle $\alpha$ and the direction of the line from point 1 to point 2, one could reconstruct the initial photon direction, provided that the scattering plane is well constrained. Otherwise, in the absence of information on the orientation of the plane of scattering, there remains a residual uncertainty in the direction of the initial photon: it could come anywhere from a cone with the axis along 1-2 direction and the opening angle $\theta$. The orientation of the plane of scattering could, in principle, be constrained if the direction of motion of the electron scattered at point 1 is measured. However, this is usually challenging because the electron immediately experiences miltiple scattering in the detector volume and quickly looses the "memory" of its initial direction. In this way, the measurements of the directions of photons detected by Compton telescopes are usually not spots on the sky, but rather "rings on the sky".

The only space-based Compton telescope which was operational up to now was COMPTEL on board of Compton Gamma-Ray Ob-

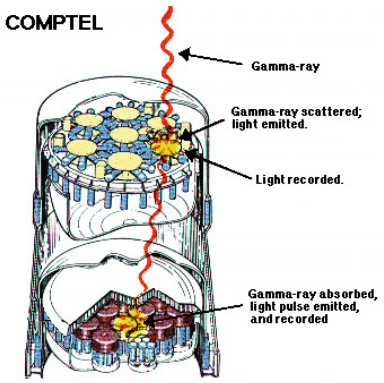


Figure 2.11: COMPTEL telescope which was operational on Compton Gamma-Ray Observatory

servatory mission by NASA. It was operation in the 90th of the last century. The setup of the telescope is shown in Fig. 2.11. In the COMPTEL setup the "scatterer" and "absorber" detectors (containing, respectively, the scattering point 1 and the absorption point 2) were separated by a distance of about 1 m onto two sub-detectors. Both sub-detectors were scintillators (liquid scintillator for the scatterer and NaI crystals for the lower absorber detector). The large separation between the sub-detectors was necessary for suppression of the background of up-going particles from the direction of the Earth. The up-going particles were rejected based on the "time-of-flight" measurement principle: they produced first signal in the "absorber" and second signal in the "scatterer", while the $\gamma$-rays from the sky produced first the signal in the "scatterer" and then in the "absorber".

The separation of the two detectors, although useful for the background rejection, strongly reduced the efficiency of the telescope. Large fraction of the scattered $\gamma$-rays just did not arrive at the lower detector. Because of this, COMPTEL had a limited sensitivity and detected only about 10 sources on the sky. Our lack of sensitive instruments (and knowledge) in the MeV energy domain is known as the "MeV sensitivity gap". Telescopes operating in adjacent energy bands (below 100 keV and above 100 MeV are much more sensitive and our knowledge of the sky in those energy bands is much more complete.

## 2.8 Inverse Compton scattering

Up to now we have considered scattering of photons by electron at rest. In this case it is the photon which transfers a fraction of its energy to electron. If electrons are moving, opposite is also possible: electron could transfer a fraction of its energy to photon. In this case Compton scattering works as a radiative energy loss for high-energy electrons. This process is called inverse Compton scattering. Below we derive necessary formulae describing this radiative energy loss.

### 2.8.1 Energies of upscattered photons

The case of arbitrary initial four-momentum of electron could be reduced to the case of electron in rest via a transformation to the coordinate system comoving with the electron. Suppose that electron moves with velocity $v$ along $x$ axis in the "lab" frame. In the same frame photon moves at an angle $\theta_0$ w.r.t. electron and its four-momentum is $\underline{p}_{\gamma,i} = \epsilon_i(1, \cos\theta_0, \sin\theta_0, 0)$. Lorentz transformation of photon four-momentum to the electron comoving frame changes the energy as

$$\tilde{\epsilon}_i = \epsilon_i\gamma(1 - v\cos\theta_0) \tag{2.98}$$

where $\gamma$ is the Lorentz factor of electron. The final energy of scattered photon in the comoving frame is

$$\tilde{\epsilon}_f = \frac{\tilde{\epsilon}_i}{1 + \frac{\tilde{\epsilon}_i}{m_e}(1 - \cos\alpha')} \tag{2.99}$$

where $\alpha'$ is the scattering angle in the comoving frame. The final photon energy in the lab frame is related to $\tilde{\epsilon}_f$ also via Lorentz transformation

$$\epsilon_f = \tilde{\epsilon}_f\gamma(1 + v\cos\theta_f) = \frac{\epsilon_i\gamma^2(1 - v\cos\theta_0)(1 + v\cos\theta'_f)}{1 + \frac{\tilde{\epsilon}_i}{m_e}(1 + \cos\alpha')} \tag{2.100}$$

where $\theta'_f$ is the angle of outgoing photon w.r.t. the $x$ axis in the comoving frame.

Now let us consider situation in which the energy of the incident photon in the electron comoving frame is small

$$\tilde{\epsilon}_i \ll m_e \tag{2.101}$$

For this to be true we have to require

$$\epsilon_i \gamma (1 - v \cos\theta_0) \ll m_e \tag{2.102}$$

which, by itself requires

$$\epsilon_i E_e \ll m_e^2 \tag{2.103}$$

where $E_e = \gamma m_e$ is the initial electron energy. Compton scattering of low-energy photons by relativistic electrons in the regime where low-energy photons satisfy condition (2.103) is called "inverse Compton scattering in Thomson regime".

In this case Eq. (2.100) simplifies and we find

$$\epsilon_f \simeq \epsilon_i \gamma^2 (1 - v \cos\theta_0)(1 + v \cos\theta'_f) \tag{2.104}$$

Now assume that the low energy photons form an isotropic radiation field and the angle $\theta_0$ is random. In the electron comoving frame, the scattering amplitude is comparable in all the directions, so that the angle $\theta'_f$ also takes arbitrary values. This means that a good estimate of the average final energy of photons is

$$\epsilon_f \simeq \epsilon_i \gamma^2 \simeq 3 \left[\frac{\epsilon_i}{1 \text{ eV}}\right] \left[\frac{E_e}{10^{10} \text{ eV}}\right]^2 \text{ GeV} \tag{2.105}$$

Thus, contrary to the scattering of waves on electron at rest, where the scattering process took the energy from the wave, here the energy is transferred from electron to photons and the process converts low energy photons into high energy $\gamma$-rays. Such process is called "inverse" Compton scattering.

Note that as long as condition (2.103) is satisfied, the final energy of photons $\epsilon_f$ is always

$$\epsilon_f \ll E_e \tag{2.106}$$

At each scattering event electron transfers only a small fraction of its energy to the photon.

The scattering angle is approximately arbitrary in the comoving frame. However, in the lab frame the scattering would appear strongly beamed in forward direction, within a cone with an opening angle $\gamma^{-1}$.

## 2.9 Excercises

**Excercise 2.1.** Use the expression for the intensity of radiation from a relativistically moving charge (2.16) for an order-of-magnitude comparison of contributions due to the first and second term for an ultra-relativistic particle moving with veolcity $v = 1 - \epsilon$, $\epsilon \ll 1$, experiencing acceleration on a time scale $t = 1/\omega_0$. Which term dominates: the one proportional to $a_{||}$, or the one proportional to $a_\perp$?

**Excercise 2.2.** By analogy with the astrophysical example of curvature radiation from pulsar magnetosphere, consider the possibility of curvature radiation from a magnetosphere of a black hole in an Active Galactic Nucleus (AGN) of M87 galaxy. The black hole mass is $M \sim 4 \times 10^9 M_\odot$ and the characteristic distance scale in the source is the gravitational radius $R_g$ (see. Excercise 1.4). $\gamma$-rays with energies up to 10 TeV are detected from M87 (see Fig. 2.12). Using this information find an upper bound on energies of electrons and protons present in the source. Find a characteristic curvature radiation energy loss time scale

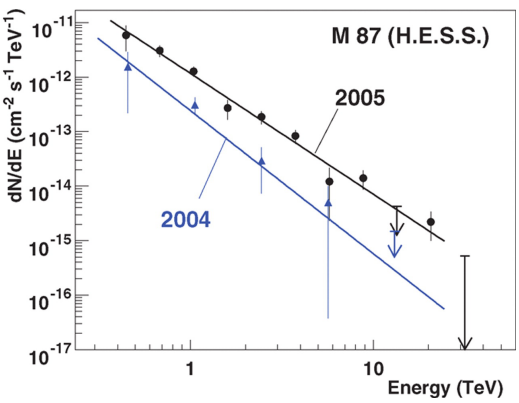

$t_{curv} = E/I_{curv}$ for electrons and protons of energy $E$. Is it shorter or longer than the "light-crossing" time scale $t_{lc} = R_g/c$?

**Excercise 2.3.** Find steady-state spectrum of high-energy particles injected at a constant rate with a powerlaw spectrum $Q_e(E) \sim E^{-\Gamma_{inj}}$ and cooling due to a radiative energy loss with the energy loss rate which scales as powerlaw of particle energy: $\dot{E} \sim E^{\gamma_{cool}}$.

**Excercise 2.4.** "Landau levels". In quantum mechanical settings, find the spectrum of energy levels for a particle of charge $e$ moving in a plane perpendicular to the direction of a homogeneous magnetic field with strength $B$.

**Excercise 2.5.** Find the slope of the powerlaw spectrum of high-energy electrons in Crab nebula, by measuring the slope of its emission spectrum in $10 - 10^8$ eV photon energy range (Fig. 2.6).

**Excercise 2.6.** Estimate the mass of objects powering active galactic nuclei assuming that these sources with typical luminosity $10^{45}$ erg/s radiate at the Eddington luminosity limit.

**Excercise 2.7.** Estimate angular resolution of Compton telescope based on given precision of measurement of energy deposits $\Delta E$ by the recoil electron and at the absorption point of the scattered photon.

## Abbreviations

| | |
|---|---|
| AGN | Active Galactic Nucleus |
| FR I, FR II | Fanaroff-Riley radio galaxy, type I or type II |
| GRB | Gamma-Ray Burst |
| HMXRB | High-Mass X-ray Binary |
| LMXRB | Low-Mass X-ray Binary |
| PSR | Pulsar (name in astronomical catalogues) |
| PWN | Pulsar Wind Nebula |
| QSO | Quasi-Stellar Object (name in astronomical catalogues) |
| SNR | Supernova Remnant |
| Sy I, Sy II | Seyfert galaxy, type I or II |
| XRB | X-Ray Binary |

# Bibliography


[1] T.Courvoisier, *High-Energy Astrophysics*, Springer 2013.

[2] M.Longair, *High-Energy Astrophysics*, Third Edition, Cambridge Univ. Press, 2011.

[3] F.Aharonian, *Very High Energy Cosmic Gamma Radiation*, World Scientific, 2004.

[4] J. Beringer et al. (Particle Data Group), Phys. Rev. D86, 010001 (2012).

[5] T.Courvoisier, A&AR, 9, 1 (1998).

[6] J.Jackson, *Classical Electrondynamics*, Wiley & Sons, 1962.

[7] L.D.Landau, E.M.Lifshitz, *The Classical Theory of Fields*, Pergamon Press, 1971.

[8] Abdo A.A. et al., Ap.J., 696, 1084, 2009.

[9] Aharonian F. et al., Science, 314, 1424, 2006.

[10] Kreykenbohm I., et al., A&A, 433, L45, 2005.

[11] Hester J.J. ARA&A, 46, 127, 2008.

[12] Tavani M. et al., Science, 331, 736, 2011.

[13] Berezinsky V., Nucl.Phys.Proc.Suppl.188, 227 (2009) [arXiv:0901.0254]

[14] Ackermann M., et al., Ap.J., 750, 3 (2012).

[15] Ackermann M., et al., Science, 334, 1103 (2011).

[16] Berger E., ARA&A, 51, 43 (2014).

[17] S.Lee, Phys.Rev. D58, 043004 (1998).

[18] K.A. Olive et al. (Particle Data Group), Chin. Phys. C, 38, 090001 (2014)

[19] Yakovelv & Petchik, ARA&A, 42, 169 (2004)